SARS-CoV-2 nsp16 is regulated by host E3 ubiquitin ligases, UBR5 and MARCHF7

Li Tian[1#], Zirui Liu[2#], Wenying Gao[1], Zongzheng Zhao[2], Xiao Li[2]*, Wenyan Zhang[1]* and Zhaolong Li[1]*

[1]Department of Infectious Diseases, Infectious Diseases and Pathogen Biology Center, Institute of Virology and AIDS Research, Key Laboratory of Organ Regeneration and Transplantation of The Ministry of Education, The First Hospital of Jilin University, Changchun 130000, Jilin, China

[2]Research Unit of Key Technologies for Prevention and Control of Virus Zoonoses, Chinese Academy of Medical Sciences, Changchun Veterinary Research Institute, Chinese Academy of Agricultural Sciences, Changchun 130000, Jilin, China

[#]These authors contributed equally to this article.

*Correspondence:

Wenyan Zhang (zhangwenyan@jlu.edu.cn), Xiao Li (skylee6226@163.com), and Zhaolong Li (lizhaolong@jlu.edu.cn)

Competing Interests: The authors declare no conflicts of interest.

Abstract

Severe acute respiratory syndrome coronavirus 2 (SARS-CoV-2), the virus responsible for coronavirus disease 2019 (COVID-19), is a global public health threat with a significant economic burden. The non-structural protein 16 (nsp16) of SARS-CoV-2, in complex with nsp10, catalyses the final step of viral mRNA capping via its 2'-O-methylase activity. This function helps the virus evade host immunity and protect viral mRNA from degradation. Current literature has not thoroughly investigated the host factors that regulate nsp16. Although various E3 ubiquitin ligases are known to interact with SARS-CoV-2 proteins, their specific roles in targeting nsp16 for degradation have not been elucidated. Here, we demonstrate that nsp16 is ubiquitinated and degraded by host E3 ubiquitin ligases UBR5 and MARCHF7, acting through the ubiquitin-proteasome system (UPS). UBR5 and MARCHF7 induce nsp16 degradation via K48- and K27-linked ubiquitination, respectively. Moreover, this degradation by either UBR5 or MARCHF7 is independent, and both processes inhibit SARS-CoV-2 replication in vitro as well as in vivo. Further, UBR5 and MARCHF7 exhibited broad-spectrum antiviral potential by degrading nsp16 variants from different SARS-CoV-2 strains. Our findings provide novel insights into the role of the UPS in antagonising SARS-CoV-2 replication and open new avenues for therapeutic interventions against COVID-19.

Key words: SARS-CoV-2, nsp16, ubiquitination, UBR5, MARCHF7, proteasomal degradation

Introduction

Severe acute respiratory syndrome coronavirus 2 (SARS-CoV-2) has emerged as a global public health threat, causing over 700 million coronavirus disease 2019 (COVID-19) cases and 7 million deaths(Carabelli et al., 2023; Markov et al., 2023). SARS-CoV-2 encodes four structural proteins, 16 non-structural proteins (Nsps) that assist in viral replication and transcription, and a series of accessory proteins (ORFs) that are associated with immune evasion (V'kovski et al., 2021; Wang et al., 2020). Some viruses, such as Ebola virus (Valle et al., 2021), dengue virus (Jung et al., 2018), and reovirus (Furuichi et al., 1975), encode 2'-O methyltransferases (2'-O-MTases) homologous to those found in eukaryotes. This allows them to mimic the host 5' cap structure on their RNA, hindering recognition by the innate immune system (Daffis et al., 2010; Züst et al., 2011). Similarly, SARS-CoV-2, in complex with nsp10, functions as a 2'-O-MTase, methylating the first nucleotide of a capped viral RNA strand at the 2′-O position, converting the 5' cap of RNA from 'cap-0' to 'cap-1' (Benoni et al., 2021; Park et al., 2022). This modification shields SARS-CoV-2 from host antiviral responses such as MDA5 recognition and IFIT1 restriction (Bergant et al., 2022; Russ et al., 2022). Importantly, nsp16 inhibits global host mRNA splicing, which reduces host protein and mRNA levels (Banerjee et al., 2020). Additionally, nsp16 enhances SARS-CoV-2 cell entry by promoting TMPRSS2 expression (Han et al., 2023), highlighting its multifaceted role as a virulence factor. Moreover, nsp16-deficient strains exhibit reduced pathogenicity and induce a strong immune response, suggesting their potential as a live-attenuated vaccine candidate (Ye et al., 2022). Given nsp16's critical functions, drugs targeting nsp16 or the nsp16-nsp10 complex have been developed (Klima et al., 2022; Nguyen et al., 2022). Therefore, understanding host factors that interact with nsp16 is crucial for uncovering novel therapeutic strategies.

The ubiquitin-proteasome system (UPS) is an important pathway for the targeted degradation of intracellular proteins and is referred to as "the molecular kiss of death" (Dongdem & Wezena, 2021; Park et al., 2020). Substrate ubiquitination requires a cascade of three ligases: E1, E2, and E3 (Zheng & Shabek, 2017). E3 ligases are

indispensable for direct binding to substrates and determining the specificity of the UPS (Li et al., 2021; Wang et al., 2022). Researchers have identified over 600 human genome-encoded E3 ligases that operate in diverse cellular environments, respond to a wide range of cellular signals, and regulate a vast array of protein substrates (Dongdem & Wezena, 2021; Garcia-Barcena et al., 2020). Dysregulation of E3 ligase activity has been implicated in various human diseases, making them promising drug targets (Humphreys et al., 2021). E3 ligases are classified into three classes based on conserved domains and ubiquitin (Ub) transfer mechanisms: Really Interesting New Gene (RING) E3s, homologous to the E6AP carboxyl terminus (HECT) E3s, and RING-between-RING (RBR) E3s (Garcia-Barcena et al., 2020; Morreale & Walden, 2016). RING E3 ligases directly transfer Ub from the E2-Ub complex to the substrate (Deshaies & Joazeiro, 2009), whereas HECT-type E3s transfer Ub to their own catalytic cystine residue before attaching it to the substrate (Huibregtse et al., 1995). RBR E3s combine the characteristics of both RING and HECT types (Walden & Rittinger, 2018). RBR and RING E3s share the RING-binding domains, but RBR family members can generate thioester intermediates with ubiquitin, as is the case with HECT-type E3s (Garcia-Barcena et al., 2020).

To revealing the relationships between SARS-CoV-2 and host factors, we focused on the mechanism of interactions between nsp16 and UPS. In this study, we present a novel regulatory mechanism against nsp16 by the host UPS. We demonstrate, for the first time, that nsp16 is ubiquitinated and degraded by the host proteasome. Interestingly, two E3 ligases from distinct families, the RING-type MARCHF7 and the HECT-type UBR5, independently recognise and target nsp16 for degradation in both the cytoplasm and nucleus. This dual targeting by MARCHF7 and UBR5 impairs the 2'-O-MTase activity of nsp16, blocking the conversion of cap-0 to cap-1 at the 5 'end of viral RNA, ultimately exhibiting potent antiviral activity against SARS-CoV-2. Our findings identify novel therapeutic targets for developing effective strategies to prevent SARS-CoV-2 and treat COVID-19.

Results

Ubiquitination and proteasomal degradation of SARS-CoV-2 nsp16 by the UPS

Ubiquitination plays an important role in SARS-CoV-2 infection and pathogenesis (Gao et al., 2022; Guo et al., 2021; Li et al., 2023; Zhang et al., 2021; Zhang et al., 2024; Zhang et al., 2023). To explore whether the non-structural proteins of SARS-CoV-2 are regulated by the UPS, we examined the effect of the proteasome inhibitor MG132 on the protein expression of all 16 non-structural proteins and found that MG132 treatment markedly increased the abundance of nsp8, nsp11, and nsp16 proteins (Fig. 1A) in HEK293T cells. This suggests their potential degradation by the UPS. In this study, we focused on nsp16 for further investigation. To confirm the role of the UPS in nsp16 degradation, we employed additional proteasome inhibitors, Bortezomib and Carfilzomib. These inhibitors, unlike the lysosomal inhibitors Bafilomycin A1 and NH_4Cl and the autophagy-lysosomal inhibitor vinblastine, enhanced nsp16 stability (Fig. 1B). The effect of USP on the half-life of nsp16 was investigated. To this end, nsp16-expressing cells were treated with a protein synthesis inhibitor, cycloheximide, and the kinetics of nps16 decay were examined. We observed that the half-life of nsp16 in MG132-treated samples was significantly longer than in MG132-untreated samples (15 h versus 2 h) (Fig. 1C and 1D).

Next, we enriched the nsp16 protein by co-immunoprecipitation (Co-IP) and analysed the nsp16-interacting proteins by comparing the differential proteins between nsp16 cells treated with and without MG132 using mass spectrometry (MS) (Fig. 1E). Based on the results obtained by MS, KEGG pathway and gene ontology analyses were performed (Figure 1—figure supplement 1A). Biological process enrichment analysis showed that blocking nsp16 degradation resulted in an increase in the number of proteins that interact with nsp16, including 43 proteins involved in virus-associated processes and 22 proteins involved in regulating mRNA stability. Five proteins were related to the regulation of the cellular defence response to the virus. In addition to stability, proteins interacting with nsp16 are also associated with mRNA splicing and RNA methylation (Banerjee et al.,

2020). It is well known that nsp16 is a 2'-O-MTase involved in 5-capping of mRNA to stabilise the RNA and prevent its recognition by MDA5 and IFIT1 in the cell for immune escape. Furthermore, SARS-CoV-2 uses nsp16 to disrupt host mRNA splicing to facilitate its infection (Park et al., 2022; Russ et al., 2022; Züst et al., 2011). These reported interactions confirm the reliability of our MS data.

As expected, we found that several nsp16-binding proteins were related to ubiquitination and degradation pathways (Figure 1—figure supplement 1B). Four deubiquitinases (DUBs), the E2 ligase UBE2D3, and 14 proteasomal enzymes were identified. Of these, six E3 ligases, UBR5, MARCHF7, HECTD1, TRIM32, MYCPB2, and TRIM21, were chosen for further investigation.

E3 ligases UBR5 and MARCHF7 independently mediate nsp16 degradation

To identify the E3 ligases responsible for nsp16 degradation, we designed small interfering RNA (siRNA) targeting the six E3 ligases and evaluated the effects of each E3 ligase knockdown on nsp16 abundance. Knockdown of UBR5 and MARCHF7 stabilised the protein levels of nsp16 (Fig. 2A). Furthermore, we generated stable cell lines with UBR5 and MARCHF7 knockdowns to further investigate their effects on nsp16 stability and silencing efficiency (Fig. 2B). To determine if UBR5 and MARCHF7 cooperate in nsp16 degradation, we knocked down UBR5 or MARCHF7 using siRNA in MARCHF7- or UBR5-silenced cells, respectively. Knockdown of UBR5 in MARCHF7-silenced cells, and vice versa, further enhanced nsp16 stability. This indicates that UBR5 and MARCHF7 act independently to degrade nsp16 (Fig. 2C). We further validated the independent function of these E3 ligases by examining nsp16 degradation. MARCHF7 overexpression in either MARCHF7 knockdown or MARCHF7/UBR5 double knockdown cells showed that MARCHF7 could induce nsp16 degradation in both instances. Similarly, UBR5 overexpression was also able to degrade nsp16, even in the presence of MARCHF7 knockdown. The knockdown efficiency was confirmed for all experiments (Figure 2—figure supplement 1A and 1B). Importantly, overexpression of wild-type MARCHF7, but

not a RING domain-deletion mutant lacking amino acids (aa) 1–542, destabilised nsp16 in both MARCHF7 and UBR5 knockdown cells (Fig. 2D and 2E). These results suggest that UBR5 and MARCHF7 independently ubiquitinate nsp16, targeting it for proteasomal degradation via their RING domains.

UBR5 and MARCHF7 directly interact and colocalise with nsp16 in the endoplasmic reticulum

As confirmed by MS, both Myc-tagged MARCHF7 and endogenous UBR5 interact with nsp16, as seen in the Co-IP experiment (Figure 3—figure supplement 1A and 1B). To determine whether MARCHF7 or UBR5 directly interacts with nsp16, fluorescence resonance energy transfer (FRET) experiments were performed. When nsp16-YFP was bleached, the fluorescence signals from CFP-UBR5 or CFP-MARCHF7 fusion proteins increased, indicating a direct interaction between these E3 ligases and nsp16 (Figure 3—figure supplement 1C). Image J software was used to quantify the relative fluorescence intensities (Figure 3—figure supplement 1D). We next investigated whether UBR5 and MARCHF7 require each other for nps16 binding. We compared the binding ability of UBR5 to nsp16 in the presence or absence of MARCHF7 by Co-IP. MARCHF7 knockdown had no effect on the interaction between UBR5 and nsp16, and vice versa (Fig. 3A and 3B). These results suggest independent binding of UBR5 and MARCHF7 to nsp16. Previous studies have shown that nsp16 is localised in both the nucleus and cytoplasm (Zhang et al., 2020). UBR5 (containing two nuclear localisation signals) and MARCHF7 are present in both compartments (Muñoz-Escobar et al., 2015; Shearer et al., 2018) (Nathan et al., 2008). Immunofluorescence staining revealed that UBR5 and MARCHF7 colocalised primarily with nsp16 in the cytoplasm, with some colocalisation in the nucleus of Hela cells (Figure 3—figure supplement 1E). Similar results were observed in nsp16-transfected 293T cells using antibodies against endogenous UBR5 or MARCHF7 (Figure 3—figure supplement 1F).

To determine the specific cellular compartment where MARCHF7 or UBR5 interact with nsp16, we co-transfected cells with MARCHF7-CFP or UBR5-CFP along with nsp16-YFP. Specific antibodies were used to label the mitochondrial marker COX5A, the endoplasmic reticulum (ER) marker PDI, and the Golgi apparatus marker GM130. Interestingly, both UBR5 and MARCHF7 interacted with nsp16 and colocalised with the ER marker PDI, but not with markers for mitochondria or the Golgi apparatus (Fig. 3C and 3D). These results indicate that UBR5 and MARCHF7 directly interact with nsp16 within the ER.

UBR5 and MARCHF7 mediate distinct Ub linkages on nsp16

We first confirmed that nsp16 undergoes ubiquitination (Fig. 4A). Next, we examined the effect of each E3 ligase knockdown on the overall ubiquitination level of nsp16. We observed that knockdown of either UBR5 or MARCHF7 decreased the ubiquitination level of nsp16 compared to the negative control (Fig. 4B). Ub contains seven lysine residues, which can be linked together to form polyubiquitin chains with different functions, ultimately dictating the fate of the attached protein (Grice & Nathan, 2016). To investigate the specific type of polyubiquitin chain modification of nsp16 mediated by the two E3 ligases, we constructed a series of Ub mutants containing only a single remaining lysine residue (K6, K11, K27, K29, K33, K49, and K63). Interestingly, all single-lysine Ub mutants promoted nsp16 ubiquitylation to varying degrees, indicating a complex polyubiquitin chain structure on nsp16 potentially regulated by multiple E3 ligases (Fig. 4C). However, when we analysed specific linkages, we observed that MARCHF7 knockdown primarily reduced the K27-linked ubiquitination of nsp16, while UBR5 knockdown primarily reduced the K48-linked ubiquitination of nsp16 (Fig. 4D and 4E). These findings indicate that MARCHF7 and UBR5 induce K27- and K48-linked ubiquitination on nsp16, respectively.

Functional domains of UBR5 and MARCHF7 are required for nsp16 interaction and ubiquitination

UBR5 is a four-domain E3 ligase containing two nuclear localisation signals. The four domains are UBA, UBR, PABC, and HECT (Muñoz-Escobar et al., 2015) (Figure 4—figure

supplement 1A). Notably, the HECT domain is essential for its E3 ligase activity, where UBR5 must be physically conjugated with Ub before transferring it to the substrate (Kim et al., 2021). To identify the UBR5 domain responsible for nsp16 ubiquitination, we utilised plasmid-expressing UBR5 mutants with inactivated individual domains. Interestingly, only the HECT domain mutant failed to degrade nsp16 (Figure 4—figure supplement 1B), consistent with previous studies (Zhou et al., 2022). Additionally, only this mutant lacked the ability to induce nsp16 ubiquitination, further supporting its essential function (Figure 4—figure supplement 1C).

To identify the MARCHF7 region responsible for nsp16 degradation, we constructed a series of truncation mutants, as previously described (Figure 4—figure supplement 1D) (Zhao et al., 2018) (Nathan et al., 2008). All mutants lost the ability to degrade nsp16 (Figure 4—figure supplement 1E). To investigate this observation, we explored the ability of these mutants to interact with nsp16 and their effect on nsp16 ubiquitination. Only the mutant with an intact N-terminal region (aa 1–542) retained strong binding to nsp16, while that with an intact active region of the RING domain (aa 543–616) did not. Furthermore, only the wild-type MARCHF7 induced the formation of K27-linked Ub chains on nsp16 (Figure 4—figure supplement 1F). These findings suggest that the N-terminal mediates binding to nsp16, while the RING domain is required for its K27-linked ubiquitination activity.

UBR5 and MARCHF7 mediate antiviral activity against SARS-CoV-2 by targeting nsp16 for degradation

To examine the functional impact of nsp16 degradation by UBR5 and MARCHF7 on viral replication, we used a biosafety level 2 cell culture system to generate viral SARS-CoV-2 transmissible virus-like particles capable of infecting and replicating in Caco2-N^{int} cells (Ju et al., 2021). Knockdown of either UBR5 or MARCHF7 in these cells led to a significant increase in SARS-CoV-2 levels compared to the control group. Notably,

simultaneous knockdown of both UBR5 and MARCHF7 further increased SARS-CoV-2 replication (Figure 5—figure supplement 1A and 1B).

We further validated the antiviral effects of MARCHF7 and UBR5 in a biosafety level 3 laboratory using the SARS-CoV-2 Wuhan strain with a multiplicity of infection (MOI) of 0.01 or the Omicron strain with a MOI of 0.001. Compared to the control group, MARCHF7 or UBR5 knockdown in Caco2 cells significantly increased intracellular and secreted viral mRNA levels (*M* and *E* genes) of both strains, along with increased viral titres in the supernatant (Fig. 5A–C for the Wuhan strain and 5D–F for the Omicron strain). Immunoblotting (IB) confirmed these findings, demonstrating elevated N protein levels in both the cells and supernatant upon E3 ligase knockdown (Fig. 5G). The knockdown efficiency of MARCHF7 and UBR5 was also confirmed (Fig. 5H). Due to low transfection efficiency in Caco2 cells, we overexpressed MARCHF7-Myc or UBR5-Myc in 293T cells, stably expressing the ACE2 receptor. Overexpression of MARCHF7 or UBR5 significantly decreased viral mRNA levels of the *M* and *E* genes for both the Wuhan and Omicron strains, as measured by real-time quantitative polymerase chain reaction (RT-qPCR). IB analysis also showed decreased N protein levels in cells and the supernatant, along with decreased viral titres. However, co-transfection with increasing amounts of nsp16 significantly abrogated the inhibitory effects of MARCHF7 or UBR5 on SARS-CoV-2 replication (Fig. 6A–H and Figure 6—figure supplement 1A–H). These results indicate that UBR5 and MARCHF7 significantly inhibit SARS-CoV-2 replication, and this antiviral activity is strongly linked with their ability to modulate nsp16 levels via degradation.

UBR5 and MARCHF7 mediate broad-spectrum degradation of nsp16 variants

Given the ongoing emergence of SARS-CoV-2 variants, broad-spectrum antiviral activity is important. To investigate the broad-spectrum degradation of different nsp16 variants by UBR5 and MARCHF7, we aligned the amino acid sequences of various nsp16 proteins obtained from the National Center for Biotechnology Information (Figure 6—figure supplement 2A). We found only three variants exhibited a higher number of

mutation sites, namely XBB.1.9.1, XBB.1.5, and XBB.1.16, compared to other variants with only one or two mutation sites, suggesting a more conserved sequence. Therefore, we synthesised the nsp16 sequences of these three variants along with several single-site mutants from other variants using mutagenesis techniques. Treatment with MG132, a proteasome inhibitor, restored the nsp16 proteins from all variants (Figure 6—figure supplement 2B). Furthermore, knockdown of either UBR5 or MARCHF7 increased the stability of nsp16 proteins from various variants to varying degrees. This indicates that these nsp16 proteins are sensitive to UBR5- or MARCHF7-mediated degradation (Figure 6—figure supplement 2C). Taken together, these results suggest that UBR5 and MARCHF7 may have broad-spectrum antiviral activity against SARS-CoV-2 variants by targeting nsp16 for degradation.

SARS-CoV-2 infection decreases UBR5 and MARCHF7 expression

To explore the relationship between the expression levels of UBR5 and MARCHF7 and viral load after SARS-CoV-2 infection, we detected changes in the mRNA and protein levels of UBR5 and MARCHF7 after infection with Wuhan or Omicron strains at varying MOIs using RT-qPCR and IB analysis. Both mRNA and protein levels of MARCFH7 decreased with increasing viral titres. Interestingly, UBR5 expression first increased at low titres, then continuously declined with increasing titres (Figure 6—figure supplement 3A-3C). Previous studies have reported a role for UBR5 in regulating interferon-γ-mediated pathways, which might explain the observed increase in UBR5 expression at low titres (Wu et al., 2022). To confirm this, we examined the mRNA levels of UBR5 and MARCHF7 *in vivo* following SARS-CoV-2 infection. Peripheral blood mononuclear cells were collected from SARS-CoV-2-infected patients with varying disease severity. We found a negative correlation between UBR5 mRNA levels and disease progression, while MARCHF7 had no significant correlation with disease severity (Figure 6—figure supplement 3D). These results suggest that SARS-CoV-2 may target or evade the host

cell's antiviral defences mediated by UBR5 and MARCHF7.

UBR5 and MARCHF7 protect mice from SARS-CoV-2 challenge

Since no known activators or inhibitors of E3s exist, we developed a novel method to achieve transient overexpression of these proteins in mice. This method involves high-pressure tail vein injection of plasmids (Bonamassa et al., 2011). We next investigated the *in vivo* antiviral effects of MARCHF7 and UBR5 against SARS-CoV-2 infection. Mice were injected with plasmids encoding either E3 ligase followed by SARS-CoV-2 challenge (Fig. 7A). Both MARCHF7 and UBR5 overexpression resulted in a significant decrease in viral *E* gene copy number in mouse lungs compared to the control group (Fig. 7B). In addition, injection of E3 plasmids resulted in reduced weight loss in infected mice (Fig. 7D). Histopathological analysis of major organs at 5 days post-infection showed that lungs from mice treated with MARCHF7 or UBR5 displayed attenuated lesions, including alveolar contraction and pulmonary oedema, compared to those typically observed in control mice (Fig. 7E). Treatment with MARCHF7 or UBR5 also reduced the abundance of N proteins (Fig. 7F). Collectively, these results suggest that MARCHF7 and UBR5 overexpression inhibit SARS-CoV-2 virulence *in vivo* by promoting nsp16 protein *degradation*.

SARS-CoV-2 infection can trigger a severe cytokine storm, thought to be responsible for high mortality (Song et al., 2020) (Hojyo et al., 2020). We therefore examined the levels of interleukin-6, intereukin-1 receptor antagonist, and interleukin-1 β, chemokines known to be elevated in the spleens of SARS-CoV-2-infected mice (Makaremi et al., 2022) (Hu et al., 2021). Importantly, treatment with MARCHF7 or UBR5 significantly reduced the production of these chemokines (Fig. 7G).

Discussion

SARS-CoV-2 nsp16 acts as a 2'O-MTase and catalyses the methylation of the penultimate nucleotide of the viral RNA cap to form a 5'-RNA cap structure similar to that of mammals, thereby avoiding host recognition and immune responses (Lin et al., 2020) (Balieiro et al., 2022; Russ et al., 2022). High-resolution structures of nsp16 and nsp16-nsp10 heterodimers have been analysed (Rosas-Lemus et al., 2020) (Klima et al., 2022; Lugari et al., 2010), and antiviral drugs targeting these heterodimers have been developed (Balieiro et al., 2022; Melo-Filho et al., 2022). However, host factors that interact with and regulate nsp16 remain largely unknown.

Previously, our team and others have demonstrated the importance of the UPS in regulating SARS-CoV-2 infection (Xu et al., 2022). For example, host E3 ligases, such as RNF5, Cullin4-DDB1-PRPF19, ZNF598, and TRIM7, modify and regulate key proteins of SARS-CoV-2 for degradation, thereby affecting viral replication (Li et al., 2023; Liang et al., 2022; Maimaitiyiming et al., 2022; Zhang et al., 2024). In contrast, SARS-CoV-2 utilises DUBs to reverse this process and facilitate its replication (Chen et al., 2024; Gao et al., 2024; Gao et al., 2022; Guo et al., 2021). Here, we show that nsp16 is a short-lived protein with a half-life of only 2 to 3 h targeted for ubiquitination and degradation by the UPS. Using MS and bioinformatics screening, we identified two E3 ligases, UBR5 and MARCHF7, that specifically interact with and target nsp16 for ubiquitination and degradation.

UBR5 belongs to the family of UBR box proteins and contains a HECT domain (Kim et al., 2021). UBR5 affects tumour growth and metastasis (Xiang et al., 2022) (Qiao et al., 2020) and plays diverse roles in viral infections. For example, URB5 targets Middle East respiratory syndrome coronavirus ORF4b for degradation, dampening the host immune response (Zhou et al., 2022). Conversely, UBR5 acts as a cofactor for Zika virus replication by helping TER94/VCP degrade the capsid protein and expose the viral genome to the cytoplasm (Gestuveo et al.). MARCHF7 is a RING E3 Ub ligase that regulates T cell proliferation, neuronal development, inflammasomes, and tumour progression (Zheng, 2021) (Zhang et al., 2016) (Cai et al., 2022) (Zhao et al., 2018).

However, its role in viral infections remains largely unknown, with only one report identifying it as a host protein interacting with the 2C viral protein (Mahajan et al., 2021).

We further investigated the interplay between UBR5 and MARCHF7 in nsp16 degradation. Notably, these E3 ligases function independently. They directly interact with nsp16, primarily on the cytoplasmic side of the ER of the cytoplasm. Moreover, UBR5 or MARCHF7 knockdown enhanced SARS-CoV-2 replication, whereas their overexpression impaired replication. Therefore, both UBR5 and MARCHF7 act as antiviral factors that impede SARS-CoV-2 replication through nsp16 degradation.

Notably, while nsp16 possesses 18 lysine residues, pinpointing ubiquitination sites proved difficult. Based on the structure of nsp16 (Decroly et al., 2011), we constructed truncated nsp16 mutants and found that nsp16 could still be degraded to varying degrees (data not shown), suggesting that there was more than one lysine site for E3 recognition. Fortunately, MS identified lysine at position 77 (K77) of nsp16 as a ubiquitination site (data not shown). However, a nsp16 K77R mutant was still degraded by E3 ligases, although the degree of ubiquitination was reduced compared to the wild-type, indicating that K77 might be one of several potential ubiquitination sites. Therefore, we hypothesise that nsp16 undergoes ubiquitination at multiple sites and potentially also through non-canonical pathways involving non-lysine ubiquitination sites (McClellan et al., 2019). Therefore, the identification of the complete ubiquitination landscape of nsp16 requires further investigation. In addition to UBR5 and MARCHF7, other E3 ligases could also regulate nsp16 ubiquitination, which requires further study.

In this study, we identified the host E3 ligases, UBR5 and MARCHF7, which ubiquitinate and degrade the nsp16 protein of SARS-CoV-2. We showed a negative correlation between their expression levels and the degree of infection. Furthermore, we demonstrated that these ligases function as antiviral factors that significantly inhibit SARS-CoV-2 replication. Our findings pave the way for the development of novel therapeutic strategies targeting the UPS for the treatment of COVID-19.

Materials and Methods

Reagents and antibodies

The drugs used in this study were as follows: MG132 (catalog no. S2619), Bafilomycin A1 (catalog no. S1413), Bortezomib (catalog no. S1013), Carfilzomib (catalog no. S2853) and Vinblastine (catalog no. S4504) were purchased from Selleck (Houston, TX, USA). Cycloheximide (catalog no. 66-81-9) was purchased from Sigma (Saint Louis, MO, USA). The antibodies used for immunoblotting analysis (IB) were as follows: anti-UBR5 mAb (Proteintech, Rosemont, IL, USA, catalog no. 66937-1-Ig), anti-MARCHF7 mAb (Santa Cruz Biotechnology, Dallas, TX , USA, catalog no. sc-166945), SARS-CoV-2 2'-O-ribose Methytransferase Antibody (nsp16) (Cell signaling, Danvers, Massachusetts, USA, catalog no. #70811), anti-Flag mAb (Sigma, catalog no. F1804), anti-tubulin mAb (Abcam, Cambridge, Cambridgeshire, UK, catalog no. ab11323), anti-hemagglutinin (anti-HA) pAb (Invitrogen, catalog no. 71-5500), anti-Myc pAb (Proteintech, Rosemont, IL, USA, catalog no. 16286-1-AP), and anti-GFP mAb (Abcam, catalog no. ab1218). Primary antibody: anti-COX5A pAb (Sangon Biotec, Shanghai, CHN, catalog no. D261450), anti-PDI-mAb (Proteintech, catalog no. 2E6A11) and Human GM130/GOLGA2 Antibody (R&D Systems, Minneapolis, MN, USA, catalog no. AF8199) were used for immunofluorescence, and SARS-CoV-2 nucleocapsid monoclonal antibody (mAb) (GeneTex, Irvine, CA, USA, catalog no. GTX635679) were used for Immunohistochemistry. Fluorescent secondary antibodies: goat anti-Rabbit IgG (H+L) Highly Cross Adsorbed Secondary Antibody, Alexa Fluor Plus 488 (Invitrogen, catalog no. A11001), and goat anti-Rabbit IgG (H+L) Highly Cross Adsorbed Secondary Antibody, Alexa Fluor Plus 568 (catalog no. A-11011) and immunohistochemical secondary antibodies: Streptavidin-Peroxidase Anti-Rabbit IgG kit (catalog no. KIT-9706) were purchased from Invitrogen and maixin (Fuzhou, CHN) respectively.

Cell lines and viruses

The cell lines used in this study include HEK293T cells (catalog no. CRL-11268), Hela cells (catalog no.CRM-CCL-2), Caco2 cells (catalog no. HTB-37). All cell lines were purchased from American Type Culture Collection (ATCC; Manassas, VA, USA) and

tested for mycoplasma. In order to conduct virus related experiments, stable cell lines including Caco2-N^{int} (stably expressing SARS-CoV-2 N gene) and 293T-ACE2 (stably expressing ACE2) were generated in our laboratory. The cells were cultured in a cell incubator containing 5% CO2 at 37°C using Dulbecco's modified Eagle's medium (DMEM; HyClone, Logan, UT, USA) containing 10% heat-inactivated fetal calf serum (FCS, GIBCO BRL, Grand Island, NY, USA), 100 mg/ml penicillin, and 100 ug/ml streptomycin to provide nutrition. We expanded SARS-CoV-2 virus-like-particles (Wuhan-Hu-1, MN908947, Clade:19A) with high replication capacity in Caco2-N^{int} using a biosafety level-2 (BSL-2) cell culture system. The virus infecting the cells include Omicron BA. 1 strain (human/CHN_CVRI-01/2022) and SARS-CoV-2 Wuhan strain (BetaCoV/Beijing/IME-BJ05-2020, GenBank access no. MT291831.1), and mouse adapted SARS-CoV-2/C57MA14 variant (GenBank: OL913104.1) used for experiments in mice were provided by Key Laboratory of Jilin Province for Zoonosis Prevention and Control, and all experiments for virus infection were performed in Biosafety level 3 (BSL-3) cell culture system.

Plasmids

Eukaryotic expression plasmids encoding SARS-CoV-2 nsp protein were provided by Professor Wang Peihui (Shandong University). The nsp16-HA expression vector was constructed by adding HA tag at the C-terminus. UBR5 (Gnen ID: 51366) and its mutants (UBR5-ΔHECT, UBR5-ΔPABC, UBR5-ΔUBR) expression plasmids were constructed using purchased plasmids from Addgene (Watertown, MA, USA) as templates with no tag or a MYC tag at the N-terminus. The cDNA of 293T cells was used as a template to construct MARCHF7(Gene ID: 64844) and its truncated mutant with a Myc tag at the C-terminus. All the above expression plasmids were inserted into the VR1012 vector. For immunofluorescence (IF) and Fluorescence Resonance Energy Transfer (FRET) experiments, pCDNA3.1-YFP vector (catalog no. 13033) and pECFP-C1 vector (catalog no. 6076-1) were purchased from Addgene and BD (Biosciences Clontech), and MARCHF7 or UBR5 was constructed on pECFP-C1, and nsp16 was constructed on pCDNA3.1-YFP. Single point mutants of nsp16 of different virus subtypes were obtained

by point mutagenesis. Multi-site combined mutants were synthesized by Sangon Biotec Company. Human ubiquitin protein and its mutants have been previously described. Primers required for PCR were listed in Appendix Table S1.

RNA extraction and real-time quantitative PCR

We used the way of Trizol (Invitrogen, catalog no. 15596018CN) to extract RNA. The RNA was subsequently reverse transcribed using a High-Capacity cDNA Reverse Transcription kit (Applied Biosystems, Carlsbad, CA, USA, catalog no. 4368814). Finally, PrimeScript RT Master Mix (Takara, Shiga, JPN, catalog no. RR036A) and relative real-time primer were used for qPCR on an Mx3005P instrument (Agilent Technologies, Stratagene, La Jolla, CA, USA). Amplification procedure of the target fragment is as follows: predenaturation at 95°C for 2min, denaturation at 95 °C for 30s, annealing at 55 °C for 30s, and extension at 72 °C for 30s, total of 40 cycles. Real-time primer sequences used in this study were shown in appendix table S1.

Immunoblotting analysis (IB)

Cells or supernatant cultured for a certain time were collected, cell precipitates were resuspended with lysis buffer (50 mM Tris–HCl [pH 7.8], 150 mM NaCl, 1.0% NP-40, 5% glycerol and 4 mM EDTA), 4xloading buffer was added (0.08M Tris [pH 6.8], 2.0%SDS, 10% glycerol, 0.1 M dithiothreitol, and 0.2% bromophenol blue), and samples were lysed by heating at 100℃ for 30min. After removal of cell debris by centrifugation, the supernatant was taken to separate proteins of different sizes by SDS-PAGE. The proteins were transferred onto polyvinylidene fluoride (PVDF) membranes, incubated overnight with the indicated primary antibody, and after 1 hour at room temperature with HRP-conjugated secondary antibodies (Jackson Immunoresearch, West Grove, NJ, USA, catalog no. 115-035-062 for anti-mouse and 111-035-045 for anti-rabbit), the proteins were visualized through Ultrasensitive ECL Chemiluminescence Detection Kit (Proteintech, catalog no. B500024).

Stable cell line generation

We purchased the lentiviral vector pLKO.1-puro (catalog no. 8453) from Adggen.

ShRNA targeting target genes were designed and synthesized by Sangon Biotech. After annealing, it was inserted into the vector. Lentivirus was generated by transfection with shRNA (cloned in pLKO.1) or control vector, RRE, VSVG and REV, and the cells were screened with 1/1000 puromycin (3 μg/ml, Sigma, catalog no. P8833) after infection 48 hours. The knockdown efficiency was detected by RT-qPCR or IB. The shRNA target sequences used in this study are shown in appendix table S1.

RNAi

Short interfering RNA (siRNA) used in this study were purchased from RiboBio Co. Ltd. (Guangzhou, CHN). The siRNA sequences for knockdown of MARCHF7 or UBR5 are provided in appendix table S1. The siRNA was transfected into the cells by transfection reagent Lipofectamine 2000 (Invitrogen, catalog no. 11668-019), and the corresponding plasmids were transfected 24 hours later using Lipofectamine 3000 Reagent (Invitrogen, Carlsbad, CA, USA, catalog no. L3000-008). The expression of target genes was detected by RT-qPCR or immunoblotting (IB) analysis 48 hours later.

Immunoprecipitation

After 10 hours of MG132 (10 μM) treatment, the cells were harvested, resuspended in 1ml lysis buffer (50 mM Tris-HCl [pH 7.5], 150 mM NaCl, 0.5% NP-40) containing protease inhibitor (Roche, catalog no. 11697498001), placed on the shaker oscillator for 4 hours to lyse, then centrifuged to remove cell debris, and the supernatant was incubated with the antibody and protein G agarose beads (Roche, Basel, Basel-City, CH, catalog no. 11243233001) at 4°C overnight. Protein G agarose beads was washed 6-8 times with wash buffer (20 mM Tris-HCL [pH 7.5], 100 mM NaCl, 0.1 mM EDTA, and 0.05% Tween 20) at 4°C, centrifuged at 800 g for 1 min. The proteins were eluted by adding loading buffer (0.08 M Tris [pH 6.8], 2.0% SDS, 10% glycerol, 0.1 M dithiothreitol, and 0.2% bromophenol blue), the samples were boiled at 100°C for 10min to elate the proteins. The lysates and immunoprecipitations were detected by IB.

Mass spectrometry (MS)

HEK293T were transfected with SARS-CoV-2-nsp16-Flag for 36 hours, and then

harvested after 10 hours of treatment with MG132 or DMSO. Proteins were enriched by co-immunoprecipitation assay. And the elutions were analyzed by MS. MS analysis was performed by the national center for protein science (Beijing, CHN).

Immunofluorescence

At 48 hours after transfection, the solution was discarded and cells were washed twice with preheated PBS for 5min each, followed by fixation with 4% paraformaldehyde at 37°C for 10min. After three washes with PBS, permeabilized with 0.2% Triton X-100 for 5 min at 37°C, and then immediately followed by blocking with 10% fetal bovine serum at room temperature for 1 hour. The blocked cells were incubated overnight with the indicated primary antibodies. The next day, after three washes with PBS, the cells were incubated with corresponding secondary antibodies for 1 hour at room temperature in the dark. The nuclei were stained with DAPI (49,6-diamidino-2-phenylindole, Sigma, catalog no. 9542) and then stored in 90% glycerol. The fluorescence was detected by a laser scanning confocal microscope (FV 3000, Olympus, Tokyo, Japan).

Viral infectivity assay

The Caco2 cells were transfected with siRNA by Lipofectamine RNAiMAX Reagent (Invitrogen, catalog no. 13778150) to knockdown UBR5 or MARCHF7 and infected with Wuhan strain (MOI=0.01) or Omicron-BA.1 strain (MOI=0.001) at 24 hours after transfection. After two hours of infection, the Caco2 cells were cultured in fresh medium containing 2% fetal bovine serum for 48 hours. The cells and supernatants were collected. Viral levels were characterized by RT-qPCR and IB analysis of viral structural proteins. The overexpression plasmid UBR5-Myc, MARCHF7-Myc and nsp16-Flag was transfected in 293T-ACE2 by Lipofectamine 3000 Reagent and infected with virus 24 hours later.

Mouse lines and infections

BALB/C mice, 6 weeks, were purchased from Charles River Laboratories, Beijing. Mice were cultured in groups according to experimental groups. Our study examined male and female animals, and similar findings are reported for both sexes. To reduce animal suffering, all welfare and experimental procedures were carried out in strict accordance with the Guide for the Care and Use of Laboratory Animals and relevant ethical

regulations during the experiment. The mice were randomly divided into 6 groups and injected with 40 μg/500 μl MARCHF7 or UBR5 plasmids via the tail vein at high pressure. Three groups of mice were infected 50ul with SARS-CoV-2 isolates by nasal challenge at a dose of $10^{5.5}$ $TCID_{50}$/mL, three groups were not infected with virus as control, and the empty vector injection group was also used as control.

Immunohistochemical analysis

Three mice in each group, a total of 18 mice, were sacrificed after anesthesia. The lungs of mice were collected and fixed in 4% paraformaldehyde fixative. After 2 days, the lungs were progressively dehydrated through different concentrations of ethanol solution, transparently treated, soaked in xylene, and finally embedded in paraffin. Some thin sections obtained through a microtome for hematoxylin and eosin (H&E) staining. The other fraction was incubated with 3% hydrogen peroxide for 5-10 min at room temperature to eliminate endogenous peroxidase activity. SARS-CoV-2 nucleocapsid monoclonal antibody (mAb) (GeneTex, catalog no. GTX635679) and a Streptavidin-Peroxidase Anti-Rabbit IgG kit (Maixin, Fuzhou, CHN, catalog no. KIT-9706) was used to quantify the viral level in lung tissue.

Statistical analysis

The statistical analyses used in the figures have been described in detail in the figure legends. All data were expressed as mean ± standard deviations (SDs). Statistical comparisons were performed using student's t-test, one-way ANOVA, or repeated measurement ANOVA. The differences were statistically significant as follows: *$P < 0.05$, **$P < 0.01$, ***$P < 0.001$; ns is for no meaning

Ethics statement

Collection of inpatient blood was approved by the Ethics Committee of the First Hospital of Jilin University (21K105-001) in accordance with the guidelines and principles of WMA Declaration of Helsinki and the Department of Health and Human Services Belmont Report. All study participants signed an informed consent form. PBMCS were obtained from 9 COVID-19 patients with mild disease, 6 patients with severe disease, and

5 patients with critical disease (Appendix table S2). All animal experiments were approved by the ethics committee of Research Unit of Key Technologies for Prevention and Control of Virus Zoonoses, Chinese Academy of Medical Sciences, Changchun Veterinary Research Institute, Chineses Academy of Agricultural Sciences (IACUC of AMMS-11-2020-006).

Acknowledgments

We thank C.Y. Dai for providing critical reagents.

Funding information

This work was supported by funding from the National Natural Science Foundation of China (82341072, 81930062 and 82272316 to ZWY, 82341062 to LZL), the National Key R&D Program of China (2021YFC2301900 and 2301904, 2023YFC2306603), the Science and Technology Department of Jilin Province (YDZJ202301ZYTS521 and YDZJ202201ZYTS587), the Key Laboratory of Molecular Virology, Jilin Province (20102209), and Bethune Project, Jilin University (2023B03). The funding sources were involved in study design, data collection and interpretation, and the decision to submit the work for publication.

Authors' contributions

L.T.: Conceptualization; Data curation; Formal Analysis; Investigation; Methodology; Writing – original draft. Z.L.: Conceptualization; Data curation; Formal Analysis; Investigation; Methodology; Writing – review & editing; Funding acquisition. X.L., Z.Z. and W.G.: Methodology; Resources. W.Z.: Conceptualization; Formal Analysis; Funding acquisition; Methodology; Project administration; Resources; Writing – review & editing.

Data availability

The authors declare that [the/all other] data supporting the findings of this study are available within the paper [and its supplementary information files]. The mass spectrometry proteomics data have been deposited to the ProteomeXchange Consortium (http://proteomecentral.proteomexchange.org) via the iProX partner repository with the dataset identified PXD053961.

References

Balieiro, A. M., Anunciação, E. L., Costa, C. H., Qayed, W. S., & Silva, J. R. A. (2022). Computational Analysis of SAM Analogs as Methyltransferase Inhibitors of nsp16/nsp10 Complex from SARS-CoV-2. *International Journal of Molecular Sciences*, *23*(22), 13972.

Banerjee, A. K., Blanco, M. R., Bruce, E. A., Honson, D. D., Chen, L. M., Chow, A., Bhat, P., Ollikainen, N., Quinodoz, S. A., & Loney, C. (2020). SARS-CoV-2 disrupts splicing, translation, and protein trafficking to suppress host defenses. *Cell*, *183*(5), 1325-1339. e1321.

Benoni, R., Krafcikova, P., Baranowski, M. R., Kowalska, J., Boura, E., & Cahová, H. (2021). Substrate specificity of SARS-CoV-2 nsp10-nsp16 methyltransferase. *Viruses*, *13*(9), 1722.

Bergant, V., Yamada, S., Grass, V., Tsukamoto, Y., Lavacca, T., Krey, K., Mühlhofer, M. T., Wittmann, S., Ensser, A., & Herrmann, A. (2022). Attenuation of SARS-CoV-2 replication and associated inflammation by concomitant targeting of viral and host cap 2'-O-ribose methyltransferases. *The EMBO journal*, *41*(17), e111608.

Bonamassa, B., Hai, L., & Liu, D. (2011). Hydrodynamic gene delivery and its applications in pharmaceutical research. *Pharm Res*, *28*(4), 694-701. https://doi.org/10.1007/s11095-010-0338-9

Cai, B., Zhao, J., Zhang, Y., Liu, Y., Ma, C., Yi, F., Zheng, Y., Zhang, L., Chen, T., & Liu, H.

596 (2022). USP5 attenuates NLRP3 inflammasome activation by promoting autophagic
597 degradation of NLRP3. *Autophagy*, *18*(5), 990-1004.
598 Carabelli, A. M., Peacock, T. P., Thorne, L. G., Harvey, W. T., Hughes, J., 6, C.-G. U. C. d. S.
599 T. I., Peacock, S. J., Barclay, W. S., de Silva, T. I., & Towers, G. J. (2023).
600 SARS-CoV-2 variant biology: immune escape, transmission and fitness. *Nature*
601 *Reviews Microbiology*, *21*(3), 162-177.
602 Chen, X., Tian, L., Zhang, L., Gao, W., Yu, M., Li, Z., & Zhang, W. (2024). Deubiquitinase
603 USP39 promotes SARS-CoV-2 replication by deubiquitinating and stabilizing the
604 envelope protein. *Antiviral Res*, *221*, 105790.
605 https://doi.org/10.1016/j.antiviral.2023.105790
606 Daffis, S., Szretter, K. J., Schriewer, J., Li, J., Youn, S., Errett, J., Lin, T.-Y., Schneller, S., Zust,
607 R., & Dong, H. (2010). 2′-O methylation of the viral mRNA cap evades host restriction
608 by IFIT family members. *Nature*, *468*(7322), 452-456.
609 Decroly, E., Debarnot, C., Ferron, F., Bouvet, M., Coutard, B., Imbert, I., Gluais, L.,
610 Papageorgiou, N., Sharff, A., & Bricogne, G. (2011). Crystal structure and functional
611 analysis of the SARS-coronavirus RNA cap 2′-O-methyltransferase nsp10/nsp16
612 complex. *PLoS pathogens*, *7*(5), e1002059.
613 Deshaies, R. J., & Joazeiro, C. A. (2009). RING domain E3 ubiquitin ligases. *Annual review of*
614 *biochemistry*, *78*, 399-434.
615 Dongdem, J. T., & Wezena, C. A. (2021). Functional Significance of the E3 Ubiquitin Ligases
616 in Disease and Therapeutics. *Hydrolases*.
617 Furuichi, Y., Morgan, M., Muthukrishnan, S., & Shatkin, A. (1975). Reovirus messenger RNA

618 contains a methylated, blocked 5'-terminal structure: m-7G (5') ppp (5') G-MpCp.
619 *Proceedings of the National Academy of Sciences*, *72*(1), 362-366.
620 Gao, W., Wang, L., Cui, W., Wang, H., Huang, G., Li, Z., Li, G., & Zhang, W. (2024).
621 Deubiquitinase USP1 regulates sarbecovirus ORF6 protein function. *J Virol*, *98*(1),
622 e0143723. https://doi.org/10.1128/jvi.01437-23
623 Gao, W., Wang, L., Ju, X., Zhao, S., Li, Z., Su, M., Xu, J., Wang, P., Ding, Q., & Lv, G. (2022).
624 The deubiquitinase USP29 promotes SARS-CoV-2 virulence by preventing
625 proteasome degradation of ORF9b. *Mbio*, *13*(3), e01300-01322.
626 Garcia-Barcena, C., Osinalde, N., Ramirez, J., & Mayor, U. (2020). How to inactivate human
627 ubiquitin E3 ligases by mutation. *Frontiers in cell and developmental biology*, *8*, 39.
628 [Record #31 is using a reference type undefined in this output style.]
629 Grice, G. L., & Nathan, J. A. (2016). The recognition of ubiquitinated proteins by the
630 proteasome. *Cellular and molecular life sciences*, *73*, 3497-3506.
631 Guo, G., Gao, M., Gao, X., Zhu, B., Huang, J., Luo, K., Zhang, Y., Sun, J., Deng, M., & Lou, Z.
632 (2021). SARS-CoV-2 non-structural protein 13 (nsp13) hijacks host deubiquitinase
633 USP13 and counteracts host antiviral immune response. *Signal transduction and*
634 *targeted therapy*, *6*(1), 119.
635 Han, T., Lei, J., Liu, Y., Wang, Y., Xun, W., Hu, Q., Peng, Q., & Zhang, W. (2023). NSP16
636 promotes the expression of TMPRSS2 to enhance SARS-CoV-2 cell entry. *Genes &*
637 *Diseases*, *10*(3), 723-726.
638 Hojyo, S., Uchida, M., Tanaka, K., Hasebe, R., Tanaka, Y., Murakami, M., & Hirano, T. (2020).
639 How COVID-19 induces cytokine storm with high mortality. *Inflamm Regen*, *40*, 37.

640 https://doi.org/10.1186/s41232-020-00146-3

641 Hu, B., Huang, S., & Yin, L. (2021). The cytokine storm and COVID-19. *J Med Virol*, *93*(1),
642 250-256. https://doi.org/10.1002/jmv.26232

643 Huibregtse, J. M., Scheffner, M., Beaudenon, S., & Howley, P. M. (1995). A family of proteins
644 structurally and functionally related to the E6-AP ubiquitin-protein ligase. *Proceedings*
645 *of the National Academy of Sciences*, *92*(7), 2563-2567.

646 Humphreys, L. M., Smith, P., Chen, Z., Fouad, S., & D'Angiolella, V. (2021). The role of E3
647 ubiquitin ligases in the development and progression of glioblastoma. *Cell Death &*
648 *Differentiation*, *28*(2), 522-537.

649 Ju, X., Zhu, Y., Wang, Y., Li, J., Zhang, J., Gong, M., Ren, W., Li, S., Zhong, J., Zhang, L.,
650 Zhang, Q. C., Zhang, R., & Ding, Q. (2021). A novel cell culture system modeling the
651 SARS-CoV-2 life cycle. *PLoS Pathog*, *17*(3), e1009439.
652 https://doi.org/10.1371/journal.ppat.1009439

653 Jung, J. I., Han, S. R., & Lee, S.-W. (2018). Development of RNA aptamer that inhibits
654 methyltransferase activity of dengue virus. *Biotechnology letters*, *40*, 315-324.

655 Kim, J. G., Shin, H.-C., Seo, T., Nawale, L., Han, G., Kim, B. Y., Kim, S. J., & Cha-Molstad, H.
656 (2021). Signaling pathways regulated by UBR box-containing E3 ligases. *International*
657 *journal of molecular sciences*, *22*(15), 8323.

658 Klima, M., Khalili Yazdi, A., Li, F., Chau, I., Hajian, T., Bolotokova, A., Kaniskan, H. Ü., Han, Y.,
659 Wang, K., & Li, D. (2022). Crystal structure of SARS-CoV-2 nsp10–nsp16 in complex
660 with small molecule inhibitors, SS148 and WZ16. *Protein Science*, *31*(9), e4395.

661 Li, Z., Chen, S., Jhong, J.-H., Pang, Y., Huang, K.-Y., Li, S., & Lee, T.-Y. (2021). UbiNet 2.0: a

662 verified, classified, annotated and updated database of E3 ubiquitin ligase–substrate
663 interactions. *Database*, *2021*, baab010.
664 Li, Z., Hao, P., Zhao, Z., Gao, W., Huan, C., Li, L., Chen, X., Wang, H., Jin, N., & Luo, Z.-Q.
665 (2023). The E3 ligase RNF5 restricts SARS-CoV-2 replication by targeting its
666 envelope protein for degradation. *Signal Transduction and Targeted Therapy*, *8*(1),
667 53.
668 Liang, X., Xiao, J., Li, X., Liu, Y., Lu, Y., Wen, Y., Li, Z., Che, X., Ma, Y., & Zhang, X. (2022). A
669 C-terminal glutamine recognition mechanism revealed by E3 ligase TRIM7 structures.
670 *Nature Chemical Biology*, *18*(11), 1214-1223.
671 Lin, S., Chen, H., Ye, F., Chen, Z., Yang, F., Zheng, Y., Cao, Y., Qiao, J., Yang, S., & Lu, G.
672 (2020). Crystal structure of SARS-CoV-2 nsp10/nsp16 2′-O-methylase and its
673 implication on antiviral drug design. *Signal transduction and targeted therapy*, *5*(1),
674 131.
675 Lugari, A., Betzi, S., Decroly, E., Bonnaud, E., Hermant, A., Guillemot, J.-C., Debarnot, C.,
676 Borg, J.-P., Bouvet, M., & Canard, B. (2010). Molecular mapping of the RNA Cap 2′
677 -O-methyltransferase activation interface between severe acute respiratory syndrome
678 coronavirus nsp10 and nsp16. *Journal of Biological Chemistry*, *285*(43), 33230-33241.
679 Mahajan, S., Sharma, G. K., Bora, K., & Pattnaik, B. (2021). Identification of novel interactions
680 between host and non-structural protein 2C of foot-and-mouth disease virus. *J Gen*
681 *Virol*, *102*(3). https://doi.org/10.1099/jgv.0.001577
682 Maimaitiyiming, Y., Yang, T., Wang, Q. Q., Feng, Y., Chen, Z., Björklund, M., Wang, F., Hu, C.,
683 Hsu, C.-H., & Naranmandura, H. (2022). Heat treatment promotes ubiquitin-mediated

684 proteolysis of SARS-CoV-2 RNA polymerase and decreases viral load. *Research*.

685 Makaremi, S., Asgarzadeh, A., Kianfar, H., Mohammadnia, A., Asghariazar, V., & Safarzadeh,
686 E. (2022). The role of IL-1 family of cytokines and receptors in pathogenesis of
687 COVID-19. *Inflamm Res*, *71*(7-8), 923-947.
688 https://doi.org/10.1007/s00011-022-01596-w

689 Markov, P. V., Ghafari, M., Beer, M., Lythgoe, K., Simmonds, P., Stilianakis, N. I., &
690 Katzourakis, A. (2023). The evolution of SARS-CoV-2. *Nature Reviews Microbiology*,
691 *21*(6), 361-379.

692 McClellan, A. J., Laugesen, S. H., & Ellgaard, L. (2019). Cellular functions and molecular
693 mechanisms of non-lysine ubiquitination. *Open Biology*, *9*(9), 190147.

694 Melo-Filho, C. C., Bobrowski, T., Martin, H.-J., Sessions, Z., Popov, K. I., Moorman, N. J.,
695 Baric, R. S., Muratov, E. N., & Tropsha, A. (2022). Conserved coronavirus proteins as
696 targets of broad-spectrum antivirals. *Antiviral Research*, *204*, 105360.

697 Morreale, F. E., & Walden, H. (2016). Types of ubiquitin ligases. *Cell*, *165*(1), 248-248. e241.

698 Muñoz-Escobar, J., Matta-Camacho, E., Kozlov, G., & Gehring, K. (2015). The MLLE domain
699 of the ubiquitin ligase UBR5 binds to its catalytic domain to regulate substrate binding.
700 *Journal of Biological Chemistry*, *290*(37), 22841-22850.

701 Nathan, J. A., Sengupta, S., Wood, S. A., Admon, A., Markson, G., Sanderson, C., & Lehner,
702 P. J. (2008). The ubiquitin E3 ligase MARCH7 is differentially regulated by the
703 deubiquitylating enzymes USP7 and USP9X. *Traffic*, *9*(7), 1130-1145.

704 Nguyen, H. L., Thai, N. Q., & Li, M. S. (2022). Identifying inhibitors of NSP16-NSP10 of
705 SARS-CoV-2 from large databases. *Journal of Biomolecular Structure and Dynamics*,

706 1-10.

707 Park, G. J., Osinski, A., Hernandez, G., Eitson, J. L., Majumdar, A., Tonelli, M.,
708 Henzler-Wildman, K., Pawłowski, K., Chen, Z., & Li, Y. (2022). The mechanism of
709 RNA capping by SARS-CoV-2. *Nature*, *609*(7928), 793-800.

710 Park, J., Cho, J., & Song, E. J. (2020). Ubiquitin–proteasome system (UPS) as a target for
711 anticancer treatment. *Archives of pharmacal research*, *43*, 1144-1161.

712 Qiao, X., Liu, Y., Prada, M. L., Mohan, A. K., Gupta, A., Jaiswal, A., Sharma, M., Merisaari, J.,
713 Haikala, H. M., & Talvinen, K. (2020). UBR5 is coamplified with MYC in breast tumors
714 and encodes an ubiquitin ligase that limits MYC-dependent apoptosis. *Cancer*
715 *research*, *80*(7), 1414-1427.

716 Rosas-Lemus, M., Minasov, G., Shuvalova, L., Inniss, N. L., Kiryukhina, O., Brunzelle, J., &
717 Satchell, K. J. (2020). High-resolution structures of the SARS-CoV-2 2′
718 -O-methyltransferase reveal strategies for structure-based inhibitor design. *Science*
719 *signaling*, *13*(651), eabe1202.

720 Russ, A., Wittmann, S., Tsukamoto, Y., Herrmann, A., Deutschmann, J., Lagisquet, J., Ensser,
721 A., Kato, H., & Gramberg, T. (2022). Nsp16 shields SARS–CoV-2 from efficient MDA5
722 sensing and IFIT1-mediated restriction. *EMBO reports*, *23*(12), e55648.

723 Shearer, R. F., Frikstad, K.-A. M., McKenna, J., McCloy, R. A., Deng, N., Burgess, A., Stokke,
724 T., Patzke, S., & Saunders, D. N. (2018). The E3 ubiquitin ligase UBR5 regulates
725 centriolar satellite stability and primary cilia. *Molecular biology of the cell*, *29*(13),
726 1542-1554.

727 Song, P., Li, W., Xie, J., Hou, Y., & You, C. (2020). Cytokine storm induced by SARS-CoV-2.

728 *Clin Chim Acta*, *509*, 280-287. https://doi.org/10.1016/j.cca.2020.06.017

729 V'kovski, P., Kratzel, A., Steiner, S., Stalder, H., & Thiel, V. (2021). Coronavirus biology and
730 replication: implications for SARS-CoV-2. *Nature Reviews Microbiology*, *19*(3),
731 155-170.

732 Valle, C., Martin, B., Ferron, F., Roig-Zamboni, V., Desmyter, A., Debart, F., Vasseur, J.-J.,
733 Canard, B., Coutard, B., & Decroly, E. (2021). First insights into the structural features
734 of Ebola virus methyltransferase activities. *Nucleic acids research*, *49*(3), 1737-1748.

735 Walden, H., & Rittinger, K. (2018). RBR ligase–mediated ubiquitin transfer: a tale with many
736 twists and turns. *Nature structural & molecular biology*, *25*(6), 440-445.

737 Wang, M.-Y., Zhao, R., Gao, L.-J., Gao, X.-F., Wang, D.-P., & Cao, J.-M. (2020). SARS-CoV-2:
738 structure, biology, and structure-based therapeutics development. *Frontiers in cellular*
739 *and infection microbiology*, *10*, 587269.

740 Wang, R., You, X., Zhang, C., Fang, H., Wang, M., Zhang, F., Kang, H., Xu, X., Liu, Z., &
741 Wang, J. (2022). An ORFeome of rice E3 ubiquitin ligases for global analysis of the
742 ubiquitination interactome. *Genome Biology*, *23*(1), 1-21.

743 Wu, B., Song, M., Dong, Q., Xiang, G., Li, J., Ma, X., & Wei, F. (2022). UBR5 promotes tumor
744 immune evasion through enhancing IFN-γ-induced PDL1 transcription in triple
745 negative breast cancer. *Theranostics*, *12*(11), 5086.

746 Xiang, G., Wang, S., Chen, L., Song, M., Song, X., Wang, H., Zhou, P., Ma, X., & Yu, J. (2022).
747 UBR5 targets tumor suppressor CDC73 proteolytically to promote aggressive breast
748 cancer. *Cell Death & Disease*, *13*(5), 451.

749 Xu, G., Wu, Y., Xiao, T., Qi, F., Fan, L., Zhang, S., Zhou, J., He, Y., Gao, X., & Zeng, H. (2022).

750 Multiomics approach reveals the ubiquitination-specific processes hijacked by
751 SARS-CoV-2. *Signal Transduction and Targeted Therapy*, *7*(1), 312.
752 Ye, Z.-W., Ong, C. P., Tang, K., Fan, Y., Luo, C., Zhou, R., Luo, P., Cheng, Y., Gray, V. S., &
753 Wang, P. (2022). Intranasal administration of a single dose of a candidate live
754 attenuated vaccine derived from an NSP16-deficient SARS-CoV-2 strain confers
755 sterilizing immunity in animals. *Cellular & molecular immunology*, *19*(5), 588-601.
756 Zhang, H., Zheng, H., Zhu, J., Dong, Q., Wang, J., Fan, H., Chen, Y., Zhang, X., Han, X., & Li,
757 Q. (2021). Ubiquitin-modified proteome of SARS-CoV-2-infected host cells reveals
758 insights into virus–host interaction and pathogenesis. *Journal of Proteome Research*,
759 *20*(5), 2224-2239.
760 Zhang, J., Cruz-Cosme, R., Zhuang, M.-W., Liu, D., Liu, Y., Teng, S., Wang, P.-H., & Tang, Q.
761 (2020). A systemic and molecular study of subcellular localization of SARS-CoV-2
762 proteins. *Signal transduction and targeted therapy*, *5*(1), 269.
763 Zhang, L., Hao, P., Chen, X., Lv, S., Gao, W., Li, C., Li, Z., & Zhang, W. (2024). CRL4B E3
764 ligase recruited by PRPF19 inhibits SARS-CoV-2 infection by targeting ORF6 for
765 ubiquitin-dependent degradation. *mBio*, *15*(2), e0307123.
766 https://doi.org/10.1128/mbio.03071-23
767 Zhang, L., Wang, H., Tian, L., & Li, H. (2016). Expression of USP7 and MARCH7 is correlated
768 with poor prognosis in epithelial ovarian cancer. *The Tohoku journal of experimental*
769 *medicine*, *239*(3), 165-175.
770 Zhang, X., Yang, Z., Pan, T., Sun, Q., Chen, Q., Wang, P. H., Li, X., & Kuang, E. (2023).
771 SARS-CoV-2 Nsp8 suppresses MDA5 antiviral immune responses by impairing

772 TRIM4-mediated K63-linked polyubiquitination. *PLoS Pathog*, *19*(11), e1011792.
773 https://doi.org/10.1371/journal.ppat.1011792
774 Zhao, K., Yang, Y., Zhang, G., Wang, C., Wang, D., Wu, M., & Mei, Y. (2018). Regulation of
775 the Mdm2–p53 pathway by the ubiquitin E3 ligase MARCH 7. *EMBO reports*, *19*(2),
776 305-319.
777 Zheng, C. (2021). The emerging roles of the MARCH ligases in antiviral innate immunity.
778 *International Journal of Biological Macromolecules*, *171*, 423-427.
779 Zheng, N., & Shabek, N. (2017). Ubiquitin ligases: structure, function, and regulation. *Annual*
780 *review of biochemistry*, *86*, 129-157.
781 Zhou, Y., Zheng, R., Liu, D., Liu, S., Disoma, C., Li, S., Liao, Y., Chen, Z., Du, A., & Dong, Z.
782 (2022). UBR5 Acts as an Antiviral Host Factor against MERS-CoV via Promoting
783 Ubiquitination and Degradation of ORF4b. *Journal of Virology*, *96*(17), e00741-00722.
784 Züst, R., Cervantes-Barragan, L., Habjan, M., Maier, R., Neuman, B. W., Ziebuhr, J., Szretter,
785 K. J., Baker, S. C., Barchet, W., & Diamond, M. S. (2011). Ribose 2′-O-methylation
786 provides a molecular signature for the distinction of self and non-self mRNA
787 dependent on the RNA sensor Mda5. *Nature immunology*, *12*(2), 137-143.
788
789

Figure legends

Figure 1. The non-structural protein nsp16 of SARS-CoV-2 was identified that can be degraded through the proteasome pathway.

A. The non-structural proteins nsp8, nsp11 and nsp16 could be restored by the proteasome inhibitor MG132. HEK293T cells in 12-well plates were transfected with the plasmids of 16 nonstructural proteins (nsp1-16) encoded by SARS-CoV-2. Thirty-six hours later, the cells were treated with MG132 (10 μM) or DMSO for 12 h before collection. The protein level was detected by Immunoblotting (IB). Quantification of nsp protein levels relative to the control protein is shown. Data are representative of three independent experiments and shown as average ±SD (n = 3). Significance was determined by a two-tailed t-test: *P < 0.05; **P < 0.01; ***P < 0.001.

B. Proteasomal inhibitors but no other inhibitors stabilized nsp16 protein. HEK293T cells transfected with the nsp16-Flag expression vector were treated with dimethyl sulfoxide (DMSO), MG132 (10 μM), Bortezomib (10 μM), Carfilzomib (10 μM), Bafilomycin A1 (5 μM), Vinblastine (2.5 μM), or NH_4CL (2.5 μM) for 12 h prior to harvest. The cell lysates were analyzed by anti-Flag antibody.

(C-D). The half-life of nsp16 was prolonged by the proteasome inhibitor MG132. C. HEK293T cells were transfected with the nsp16-Flag-expressing plasmids. 12 hours later, the cells were treated with DMSO or MG132 (10 μM) for 12 h, then 50 μg/mL cycloheximide (CHX) was added. Cells were harvested at the indicated times to detect the level of viral protein by anti-Flag antibody. D. Quantification of nsp16 protein levels relative to tubulin at different time points is shown. Results are shown as mean ± SD (n = 3 independent experiments). ***, P < 0.001 by by a two-tailed t-test.

E. Samples were prepared for mass spectrometry, and nsp16 interacting proteins were obtained by immunoprecipitation (IP). The plasmids were transfected into HEK293T cells for 48 h. Treat cells with or without MG132 (10 μM) for 12 h prior to harvest. The whole-cell lysates were incubated with protein G agarose beads conjugated with anti-Flag antibodies and used for IB with anti-Flag antibodies to detect the nsp16 protein. Samples

enriched for proteins were analyzed by mass spectrometry.

Figure 1—figure supplement 1. Analysis of mass spectrometry results.

A. The DAVID bioinformatics website (https://david.ncifcrf.gov/tools.jsp) was used for KEGG pathway analysis and GO analysis of the differential proteins bound by nsp16 protein after treating with or without MG132. The bubble plots or circle diagram depict the results of the analysis separately. In bubble plots, a change from yellow to purple indicates a decreased p-value, while the size of the circles indicates the number of enriched genes. In the circle plot, depicting the BP (Biological process) analysis in the GO term, the length of the purple rectangle indicates the number of genes included in the term. The length of the green rectangle indicates the number of overlapping genes between the genes included in the term and the genes entered in the gene enrichment analysis, a change from deep to shallow of purple indicates a decreased p-value.

B. Schematic representation of proteins degraded by the proteasome pathway, as well as proteins associated with the proteasome in the MS enrichment analysis are shown.

Figure 2. MARCHF7 and UBR5 were identified as E3 ubiquitin ligases involves in nsp16 protein degradation.

A. Knockdown of MARCHF7 or UBR5 resulted in nsp16 restoration. HEK293T cells were transfected with siRNA of E3 ligase candidates for 24 h, followed by co-incubation with the nsp16-Flag-expressing plasmids for 48 h, lysed, and subjected to IB assay using anti-Flag antibody. RT-qPCR was conducted to determine the mRNA expression levels of E3 ligase candidates. Data are representative of three independent experiments and shown as average ± SD (n = 3). Significance was determined by a two-tailed t-test: ***P < 0.001.

B. RNA levels of UBR5 or MARCHF7 from HEK293T cells infected with lentivirus containing control or shRNA targeting UBR5 or MARCHF7 for 48 h and screened with antibiotics for 48 h. Knockdown cell lines were transfected with plasmids expressing nsp16-Flag, collected at the indicated times, and nsp16 protein levels were measured.

C. MARCHF7 and UBR5 acted separately and did not depend on each other. HEK293T cells stably expressing UBR5 shRNA or MARCHF7 shRNA were transfected with siRNA of

MARCHF7 or UBR5 for 24 h, respectively, followed by co-incubation with the nsp16-Flag-expressing plasmids for 48 h. The protein levels of nsp16 and the RNA levels of UBR5 and MARCHF7 were measured by IB and RT-qPCR, respectively.

(D-E). In HEK293T cells stably expressing UBR5 shRNA or MARCHF7 shRNA, nsp16 was degraded by overexpressed UBR5 or MARCHF7, respectively, whereas the mutant failed to degrade nsp16. The cell lysates were analyzed by anti-Flag antibody.

Figure 2—figure supplement 1. MARCHF7 and UBR5 degrade nsp16 independently.

(A-B). UBR5 siRNA was transfected into shMARCHF7 cells to knock down UBR5. After 24 hours, MARCHF7 and nsp16 expression vectors were co-transfected, and the cells were harvested 72 hours later. The levels of nsp16 were characterized by IB with anti-Flag antibody. Whether MARCHF7 was dependent on UBR5 to degrade of nsp16 was determined by further transfection of MARCHF7 siRNA into shUBR5 cells, followed by co-transfection of UBR5 and nsp16 expression vectors 24 h later. The other operations are the same as above. Data are representative of three independent experiments and shown as average ±SD (n = 3). Significance was determined by a two-tailed t-test. *P > 0.05; **P < 0.01; ***P < 0.001.

Figure 3. MARCHF7 and UBR5 directly interact with nsp16 respectively.

(A-B). The binding of MARCHF7 or UBR5 to nsp16 was not mutually dependent. The binding of nsp16 to UBR5 or MARCHF7 was identified by co-immunoprecipitation in HEK293T cells transfected siMARCHF7 or siUBR5, respectively. The immunoprecipitates and input were analyzed by IB. The knockdown efficiency was detected by RT-qPCR.

(C-D). MARCHF7 or UBR5 co-localized with nsp16 in the endoplasmic reticulum. Hela cells were co-transfected with YFP-nsp16(yellow) and CFP-UBR5(cyan) or CFP-MARCHF7(cyan). The organelles were labeled with antibodies against marker proteins of endoplasmic reticulum, Golgi apparatus and mitochondria respectively(red). The cells were analyzed by confocal microscopy(C). The ratio of colocalization was quantified by measuring the fluorescence intensities using Image J(D).

Figure 3—figure supplement 1. Interaction of MARCHF7 or UBR5 with nsp16.

A. HEK293T cells were transfected with either nsp16-Flag alone or together with MARCHF7-Myc. Thirty-six hours after transfection, the cells were treated with MG132 (10 μM) for 12 h. Cell lysates were subjected to immunoprecipitation with anti-Flag antibody. Using IB to analyze the precipitates and input.

B. HEK293T cells were transfected with nsp16-Flag. Cell lysates were subjected to immunoprecipitation with anti-UBR5 or IgG antibody.

(C-D). Hela cells were co-transfected with YFP-nsp16 and CFP-UBR5 or CFP-MARCHF7. A representative image of YFP-nsp16 (yellow) and ECFP-MARCHF7 (cyan) or ECFP-UBR5 (cyan) expressing cells before and after photobleaching the acceptor fluorophore, YFP. The region chosen for photobleaching is marked (white open box), Bars, 10um. The quantization of fluorescence brightness was analyzed by Image J. Data are representative of three independent experiments and shown as average ±SD (n = 3). Significance was determined by a two-tailed t-test. *P > 0.05; **P < 0.01; ***P < 0.001.

E. HeLa cells transfected with nsp16-Flag were analyzed by confocal microscopy. The Flag-tagged nsp16 labeled with anti-Flag antibody (red). MARCHF7 or UBR5 were labeled with endogenous antibodies (green). Cell nuclei were stained using DAPI (blue). Representative images were shown. Scale bars, 25 mm. The ratio of colocalization was quantified by measuring the fluorescence intensities using Image J.

F. nsp16 was stably transfected into HEK293T cells. The cells were analyzed by confocal microscopy. The other operations are the same as above.

Figure 4. MARCHF7 or UBR5 catalyze the formation of K-27 type or K-48 type ubiquitin chains of nsp16 respectively.

A. Nsp16 can be ubiquitinated. HEK293T cells co-transfected with ubiquitin-Myc and nsp16-Flag or transfected with nsp16-Flag alone. The cells were treated with MG132 for 12 h before collection. The whole-cell lysates were incubated with anti-Flag beads and used for IB with anti-Myc or anti-Flag antibodies to detect the polyubiquitination chain of

nsp16.

B. The level of ubiquitination of nsp16 decreased with decreasing the protein levels of MARCHF7 or UBR5. E3 was knocked down by transfection with siRNA targeting UBR5 or MARCHF7, and 24 h later ubiquitin-Myc and nsp16-Flag were co-transfected or nsp16-Flag alone. Cells were treated with MG132 for 12 h before collection. Whole cell lysates were incubated with anti-Flag beads, and polyubiquitinated chains of nsp16 were detected by IB with anti-Myc or anti-Flag antibodies.

C. Nsp16 can be modified by a variety of ubiquitin chains. HEK293T cells were transfected with either nsp16-HA alone or together with plasmids encoding various mutants of ubiquitin (K6 only, K11 only, K27 only, K29 only, K33 only, K48 only, K63 only). Thirty-six hours later, cells were treated with MG132 for 12 h. Cell lysates were then subjected to immunoprecipitation, followed by IB to analysis.

(D-E) MARCHF7 or UBR5 causes nsp16 to be modified by the K27 type or K48 type ubiquitin chain. 293T cell lines with or without MARCHF7 or UBR5 knockdown were co-transfected with plasmids encoding various mutants of ubiquitin (K6 only, K11 only, K27 only, K29 only, K33 only, K48 only, K63 only). The other experimental methods were the same as B.

Figure 4—figure supplement 1. Domains in which MARCHF7 or UBR5 functions.

A. The schematic represents UBR5 WT or mutants used in the study.

B. The HECT domain of UBR5 is required for nsp16 degradation. After co-transfection with UBR5 WT or mutants and nsp16-HA, cells were harvested 48 hours later, and cell lysates were examined by IB.

C. The HECT domain of UBR5 affects K48-type ubiquitin chain of nsp16.HEK293T cells were transfected with the assigned plasmids. After 36 hours, cells were treated with 10 μM MG132 for 12 hours, harvested, and cell lysates were incubated with protein G agarose beads conjugated with anti-HA antibodies. Cell lysates and precipitated samples were analyzed by IB.

D. The schematic represents wild-type and truncated forms of MARCHF7 used in the

study. E. Only MARCHF7 wild-type degraded nsp16. F. The N-terminal region of MARCHF7 interacted with nsp16, and only the wild type could catalyze the K27-type ubiquitin chain of nsp16.

Figure 5. Knockdown of MARCHF7 or UBR5 promotes viral replication.

MARCHF7 and UBR5 were knocked down by siRNA in Caco2 cells. 24 h after transfection, the cells were infected with Wuhan strain (MOI:0.01) (A-C) or Omicron BA.1 strain (MOI: 0.001) (D-F), respectively. 2 h post infection, the supernatant was discarded, and the cells were cultured in DMEM containing 3% fetal bovine serum for 48 h. The mRNA levels of SARS-CoV-2 *M* and *E* genes in the cells (A, D) and *E* genes in supernatant (B, E) were detected by RT-qPCR and the viral titers in supernatant (C, F) were measured. The N protein levels of Wuhan or Omicron viruses were detected by IB (G). Knock-down efficiencies of MARCHF7 and UBR5 were detected by RT-qPCR (H). Data are representative of three independent experiments and shown as average ±SD (n = 3). Significance was determined by one-way ANOVA, followed by a Tukey multiple comparisons posttest: *P < 0.05; **P < 0.01; ***P < 0.001.

Figure 5—figure supplement 1. Effect of MARCHF7 or UBR5 on SARS-CoV-2 trVLP.

(A-B). Knocking down MARCHF7 or UBR5 enhances SARS-CoV-2 trVLP infectivity. MARCHF7 or UBR5 was knocked down by siRNA in Caco2 cells with stable expression of SARS-CoV-2 N protein. Twenty-four hours later, cells were infected with SARS-CoV-2 virus-like-particles (MOI:0.1), the medium was changed two hours after infection, and the eGFP-positive cells were detected by flow cytometry 48 hours later(A). Protein content was determined by RT-qPCR(B).

Figure 6. Increased levels of nsp16 rescued viral inhibition by UBR5 or MARCHF7'

(A-H) UBR5 or MARCHF7 was transfected in 293T cells stably overexpressed with ACE2, and the increased doses of nsp16-Flag was transfected simultaneously. After 24 h, the cells were infected with Wuhan strains. The mRNA levels of *M* and *E* genes of Wuhan strain in the cells (A, D) and *E* gene in supernatant (B, E) were detected by RT-qPCR, as well as the detection of viral titers in supernatant (C, F). The N protein of the virus and the

overexpression efficiency was detected by IB (G, H). Data are representative of three independent experiments and shown as average ±SD (n = 3). Significance was determined by one-way ANOVA, followed by a Tukey multiple comparisons posttest. P > 0.05; **P < 0.01; ***P < 0.001. Figure 6—figure supplement 1 shows data related to infection with Omicron BA.1.

Figure 6—figure supplement 1. Effect of MARCHF7 or UBR5 on Omicron BA.1 infectivity.

(A-H). Showing data related to infection with Omicron BA.1. The experimental procedure was the same as Figure 6. Data are representative of three independent experiments and shown as average ±SD (n = 3). Significance was determined by one-way ANOVA, followed by a Tukey multiple comparisons posttest. P > 0.05; **P < 0.01; ***P < 0.001.

Figure 6—figure supplement 2. MARCHF7 or UBR5 have effects on mutant of nsp16 in different subtypes of SARS-CoV-2.

A. This diagram shows the mutation of nsp16 in different virus subtypes. The amino acids sequences of different SARS-CoV-2 strains were obtained from NCBI, and the amino acids sequences of nsp16 of different strains were compared by DNAMAN software.

B. Nsp16 mutants can still be regulated by MG132. The mutated nsp16 plasmids were transfected into HEK293T cells. After 36 hours of culture, cells were treated with 10 μm MG132 or DMSO, harvested 12 hours later, and cell lysates were examined by IB.

C. MARCHF7 or UBR5 can degrade nsp16 mutants. After transfecting MARCHF7 or UBR5 siRNA and the mutated nsp16 plasmids, the cells were harvested 48 h later. The cell lysates were detected by IB.

Figure 6—figure supplement 3. The expression level of MARCHF7 was negatively correlated with the viral titer, while the expression level of UBR5 was increased at low titer and decreased at high titer.

(A-C). The protein and mRNA levels of MARCHF7 or UBR5 upon infection with different

titers. Endogenous MARCHF7 and UBR5 RNA levels were detected by RT-qPCR 48 hours after infection with different titers of Wuhan strain (MOI:0, 0.0001, 0.001, 0.01) or omicron BA.1 strain (MOI:0, 0.0001, 0.001). Protein levels were examined by IB.

D. The expression level of UBR5 was negatively correlated with the severity of the disease but MARCHF7 expression levels were not. PBMC cells were extracted from common, severe and critical COVID-19 patients. RT-qPCR was used to detect the mRNA level of UBR5 or MARCHF7 in patients. Significance was determined by one-way ANOVA, followed by a Tukey multiple comparisons posttest. ns, $P > 0.05$; $^{**}P < 0.01$; $^{***}P < 0.001$.

Figure 7. In a mouse infection model, overexpression of MARCHF7 or UBR5 exerted inhibitory effects on virus.

(A-G) BLAB/C mice were injected with the corresponding plasmids at 40ug/500ul via the high-pressure tail vein, followed by nasal inoculation with 50μl SARS-CoV-2 virus at a dosage of $10^{5.5}$ TCID50/mL. Viral RNA loads in mouse lung tissues were detected by measuring the mRNA levels of the E genes by RT-qPCR (B). IB was used to detect the expression of MARCHF7 or UBR5 in the lung tissues(C). Mouse body weight was monitored during the experimental period (D). Representative images of H&E staining of lungs of mice with different treatments. Magnification, ×40. Bars, 20 μm(E). The staining of viral N proteins. Magnification, ×63. Bars, 20 μm. n =3 in each group(F). RT-qPCR was used to measure the expression of cytokines and chemokines in the spleens of mice in each group(G). Statistical significance was analyzed using a one-way analysis of variance with Tukey's multiple comparisons test. (NS, no significance, $^{*}p < 0.05$, $^{**}p < 0.01$, $^{***}p < 0.001$).

Figure 8. Schematic representation of MARCHF7 and UBR5 degrade SARS-CoV-2 nonstructural protein nsp16, thereby affecting the 5 ' cap structure of the viral RNA.

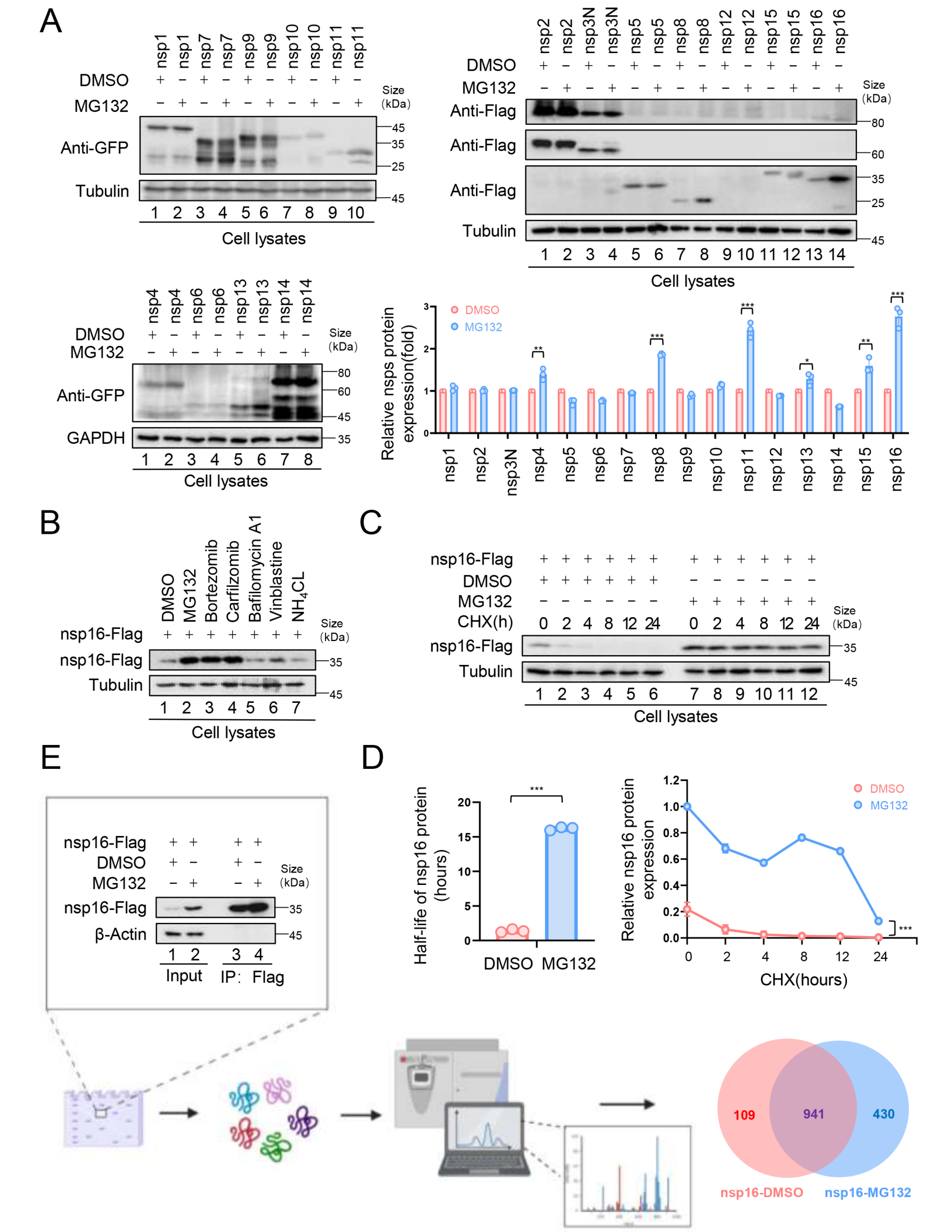
A
nsp1 nsp1 nsp7 nsp7 nsp9 nsp9 nsp10 nsp10 nsp11 nsp11
DMSO
MG132
Size (kDa)
Anti-GFP
Tubulin
45
35
25
45
1 2 3 4 5 6 7 8 9 10
Cell lysates
nsp2 nsp2 nsp3N nsp3N nsp5 nsp5 nsp8 nsp8 nsp12 nsp12 nsp15 nsp15 nsp16 nsp16
Anti-Flag
Anti-Flag
Anti-Flag
Tubulin
80
60
35
25
45
1 2 3 4 5 6 7 8 9 10 11 12 13 14
Cell lysates
nsp4 nsp4 nsp6 nsp6 nsp13 nsp13 nsp14 nsp14
GAPDH
80
60
45
35
1 2 3 4 5 6 7 8
Cell lysates
DMSO
MG132
Relative nsps protein expression(fold)
nsp1 nsp2 nsp3N nsp4 nsp5 nsp6 nsp7 nsp8 nsp9 nsp10 nsp11 nsp12 nsp13 nsp14 nsp15 nsp16
B
DMSO MG132 Bortezomib Carfilzomib Bafilomycin A1 Vinblastine NH4CL
nsp16-Flag
Size (kDa)
nsp16-Flag
Tubulin
35
45
1 2 3 4 5 6 7
Cell lysates
C
nsp16-Flag
DMSO
MG132
CHX(h) 0 2 4 8 12 24 0 2 4 8 12 24
Size (kDa)
nsp16-Flag
Tubulin
35
45
1 2 3 4 5 6 7 8 9 10 11 12
Cell lysates
E
nsp16-Flag
DMSO
MG132
Size (kDa)
nsp16-Flag
β-Actin
35
45
1 2 3 4
Input IP: Flag
D
Half-life of nsp16 protein (hours)
DMSO MG132
Relative nsp16 protein expression
DMSO
MG132
CHX(hours)
109 941 430
nsp16-DMSO nsp16-MG132

A

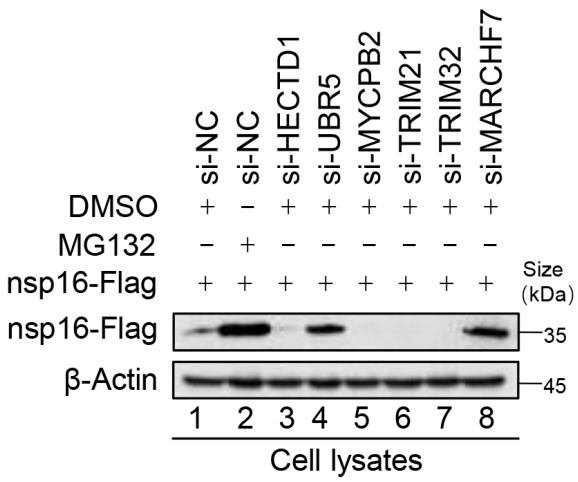
si-NC
si-NC
si-HECTD1
si-UBR5
si-MYCPB2
si-TRIM21
si-TRIM32
si-MARCHF7
DMSO
MG132
nsp16-Flag
Size (kDa)
nsp16-Flag
β-Actin
35
45
1 2 3 4 5 6 7 8
Cell lysates

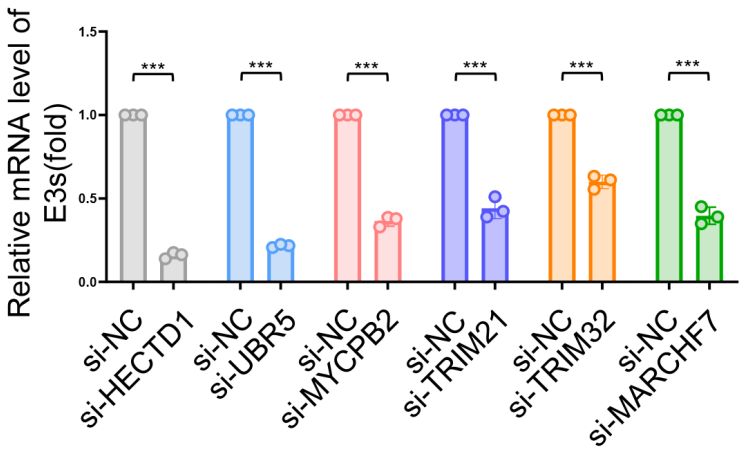
Relative mRNA level of E3s(fold)
1.5
1.0
0.5
0.0
***
si-NC
si-HECTD1
si-NC
si-UBR5
si-NC
si-MYCPB2
si-NC
si-TRIM21
si-NC
si-TRIM32
si-NC
si-MARCHF7

B

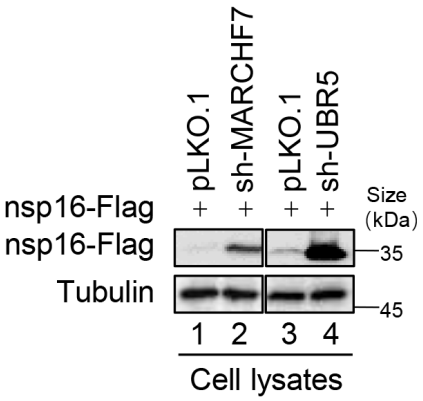
pLKO.1
sh-MARCHF7
pLKO.1
sh-UBR5
nsp16-Flag
nsp16-Flag
Tubulin
Size (kDa)
35
45
1 2 3 4
Cell lysates

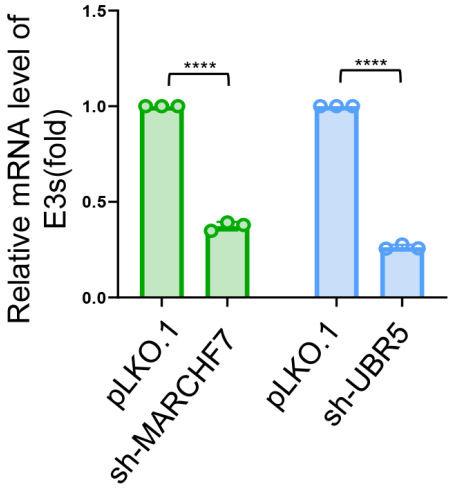
Relative mRNA level of E3s(fold)
1.5
1.0
0.5
0.0
****
pLKO.1
sh-MARCHF7
pLKO.1
sh-UBR5

C

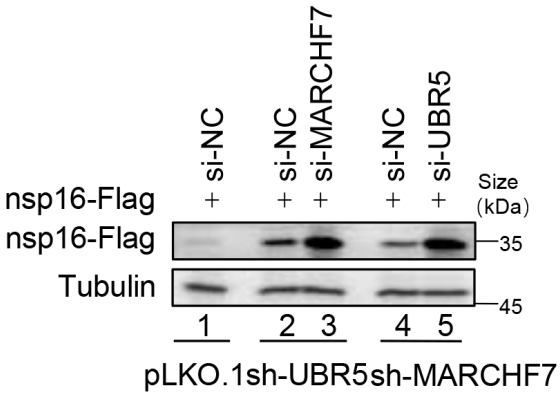
si-NC
si-NC
si-MARCHF7
si-NC
si-UBR5
nsp16-Flag
nsp16-Flag
Tubulin
Size (kDa)
35
45
1 2 3 4 5
pLKO.1sh-UBR5sh-MARCHF7

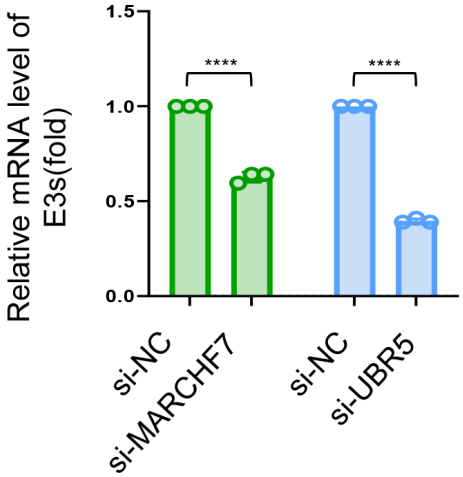
Relative mRNA level of E3s(fold)
1.5
1.0
0.5
0.0
****
si-NC
si-MARCHF7
si-NC
si-UBR5

D

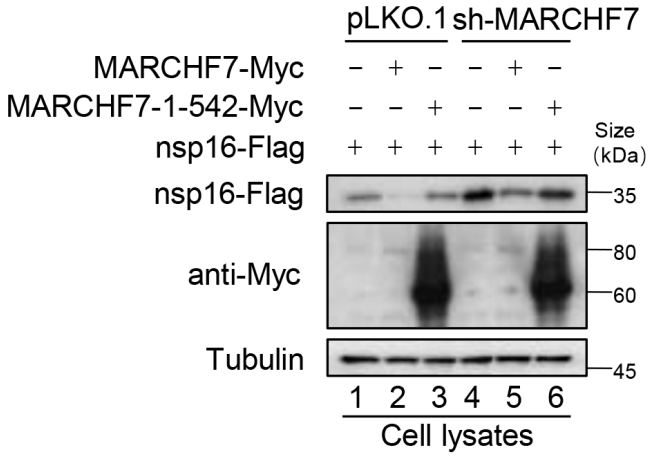
pLKO.1
sh-MARCHF7
MARCHF7-Myc
MARCHF7-1-542-Myc
nsp16-Flag
Size (kDa)
nsp16-Flag
anti-Myc
Tubulin
35
80
60
45
1 2 3 4 5 6
Cell lysates

E

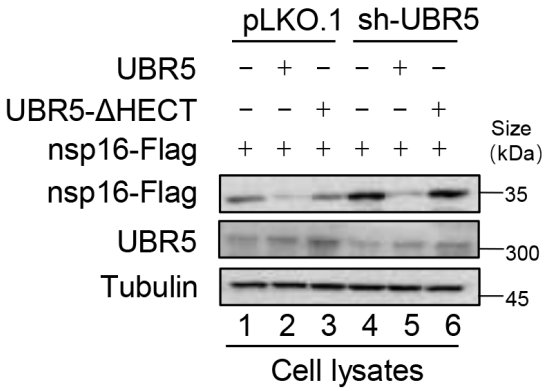
pLKO.1
sh-UBR5
UBR5
UBR5-ΔHECT
nsp16-Flag
Size (kDa)
nsp16-Flag
UBR5
Tubulin
35
300
45
1 2 3 4 5 6
Cell lysates

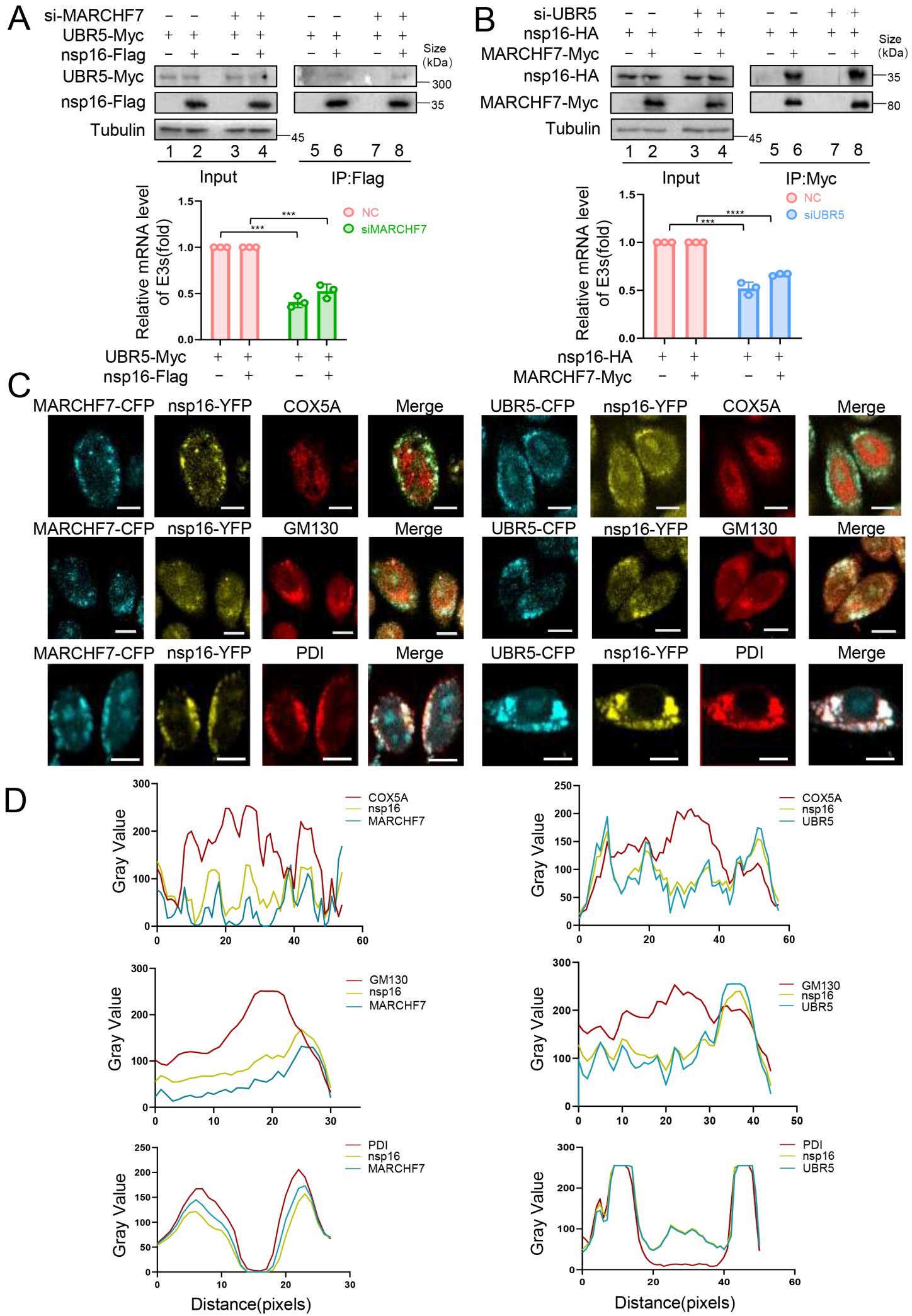
A
si-MARCHF7
UBR5-Myc
nsp16-Flag
UBR5-Myc
nsp16-Flag
Tubulin
Size (kDa)
300
35
45
1 2 3 4
5 6 7 8
Input
IP:Flag
Relative mRNA level of E3s(fold)
NC
siMARCHF7
B
si-UBR5
nsp16-HA
MARCHF7-Myc
nsp16-HA
MARCHF7-Myc
Tubulin
35
80
Input
IP:Myc
siUBR5
C
MARCHF7-CFP
nsp16-YFP
COX5A
GM130
PDI
Merge
UBR5-CFP
D
Gray Value
Distance(pixels)
COX5A
GM130
PDI
nsp16
MARCHF7
UBR5

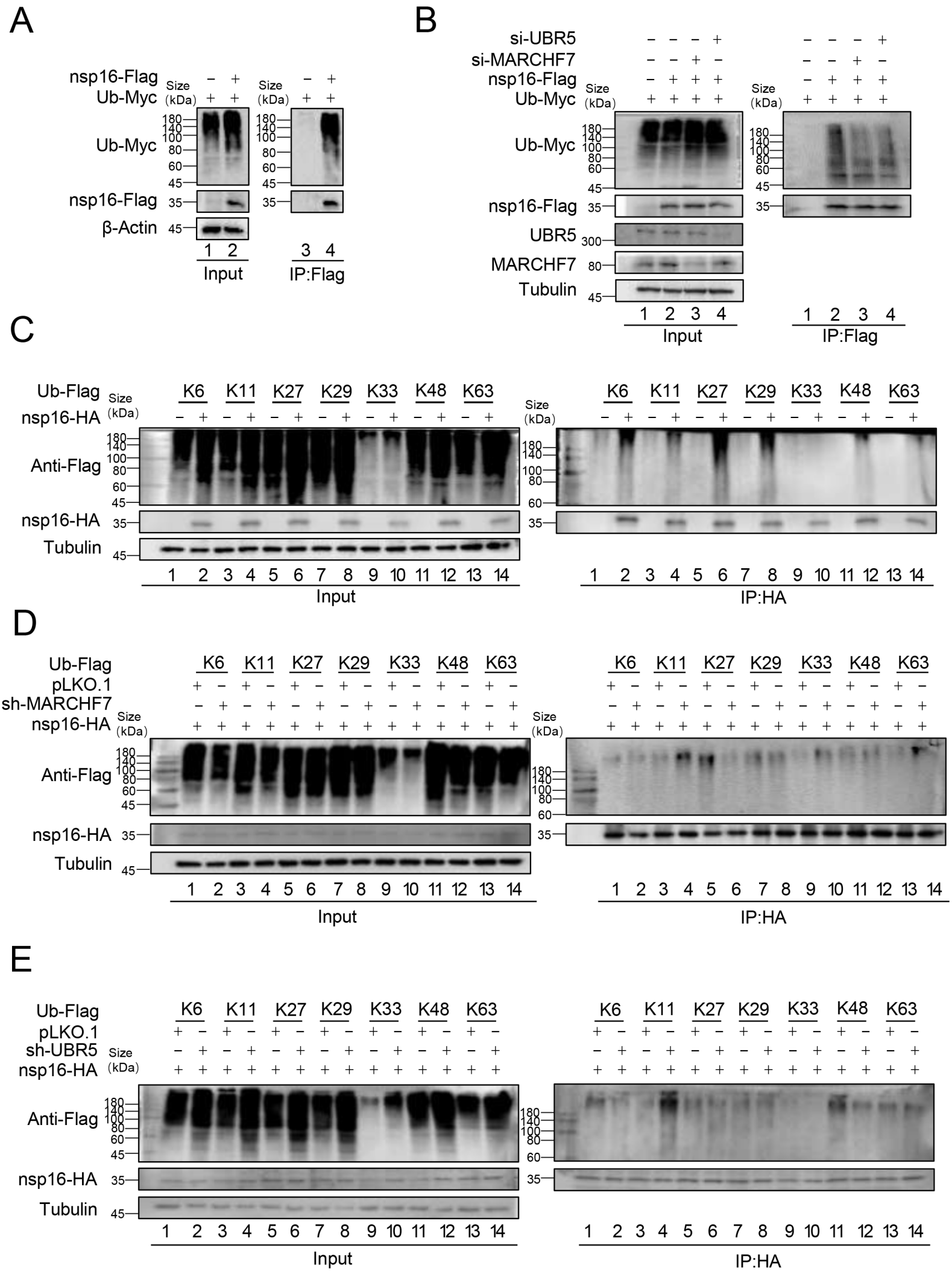
A
nsp16-Flag
Ub-Myc
Size (kDa)
Ub-Myc
nsp16-Flag
β-Actin
1 2
Input
3 4
IP:Flag
B
si-UBR5
si-MARCHF7
nsp16-Flag
Ub-Myc
Ub-Myc
nsp16-Flag
UBR5
MARCHF7
Tubulin
1 2 3 4
Input
1 2 3 4
IP:Flag
C
Ub-Flag
nsp16-HA
K6 K11 K27 K29 K33 K48 K63
Anti-Flag
nsp16-HA
Tubulin
1 2 3 4 5 6 7 8 9 10 11 12 13 14
Input
IP:HA
D
Ub-Flag
pLKO.1
sh-MARCHF7
nsp16-HA
K6 K11 K27 K29 K33 K48 K63
Anti-Flag
nsp16-HA
Tubulin
1 2 3 4 5 6 7 8 9 10 11 12 13 14
Input
IP:HA
E
Ub-Flag
pLKO.1
sh-UBR5
nsp16-HA
K6 K11 K27 K29 K33 K48 K63
Anti-Flag
nsp16-HA
Tubulin
1 2 3 4 5 6 7 8 9 10 11 12 13 14
Input
IP:HA

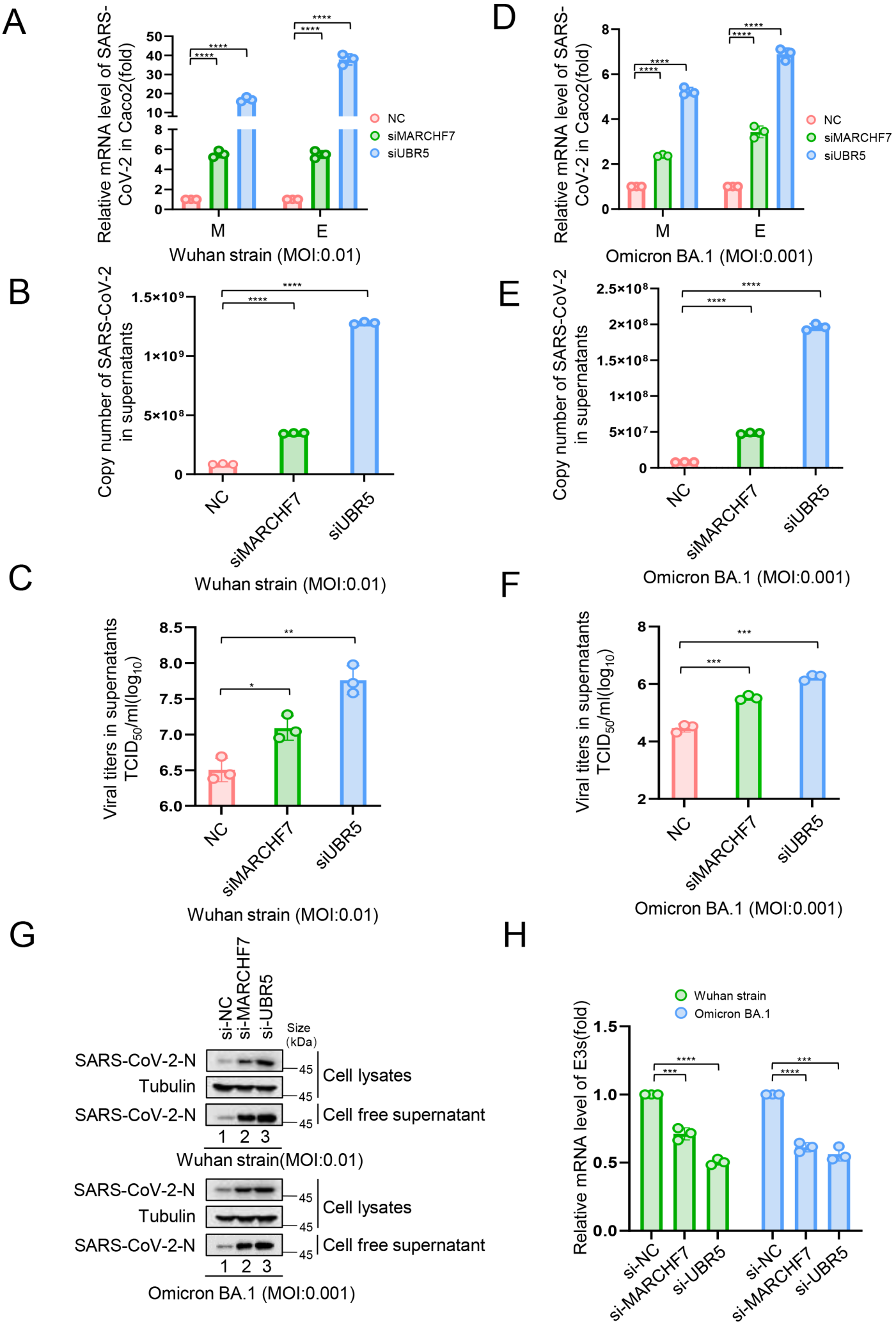
A
Relative mRNA level of SARS-CoV-2 in Caco2(fold)
NC
siMARCHF7
siUBR5
M
E
Wuhan strain (MOI:0.01)
D
Omicron BA.1 (MOI:0.001)
B
Copy number of SARS-CoV-2 in supernatants
Wuhan strain (MOI:0.01)
E
Omicron BA.1 (MOI:0.001)
C
Viral titers in supernatants TCID50/ml(log10)
Wuhan strain (MOI:0.01)
F
Omicron BA.1 (MOI:0.001)
G
si-NC
si-MARCHF7
si-UBR5
Size (kDa)
SARS-CoV-2-N
Tubulin
Cell lysates
Cell free supernatant
Wuhan strain(MOI:0.01)
Omicron BA.1 (MOI:0.001)
H
Wuhan strain
Omicron BA.1
Relative mRNA level of E3s(fold)

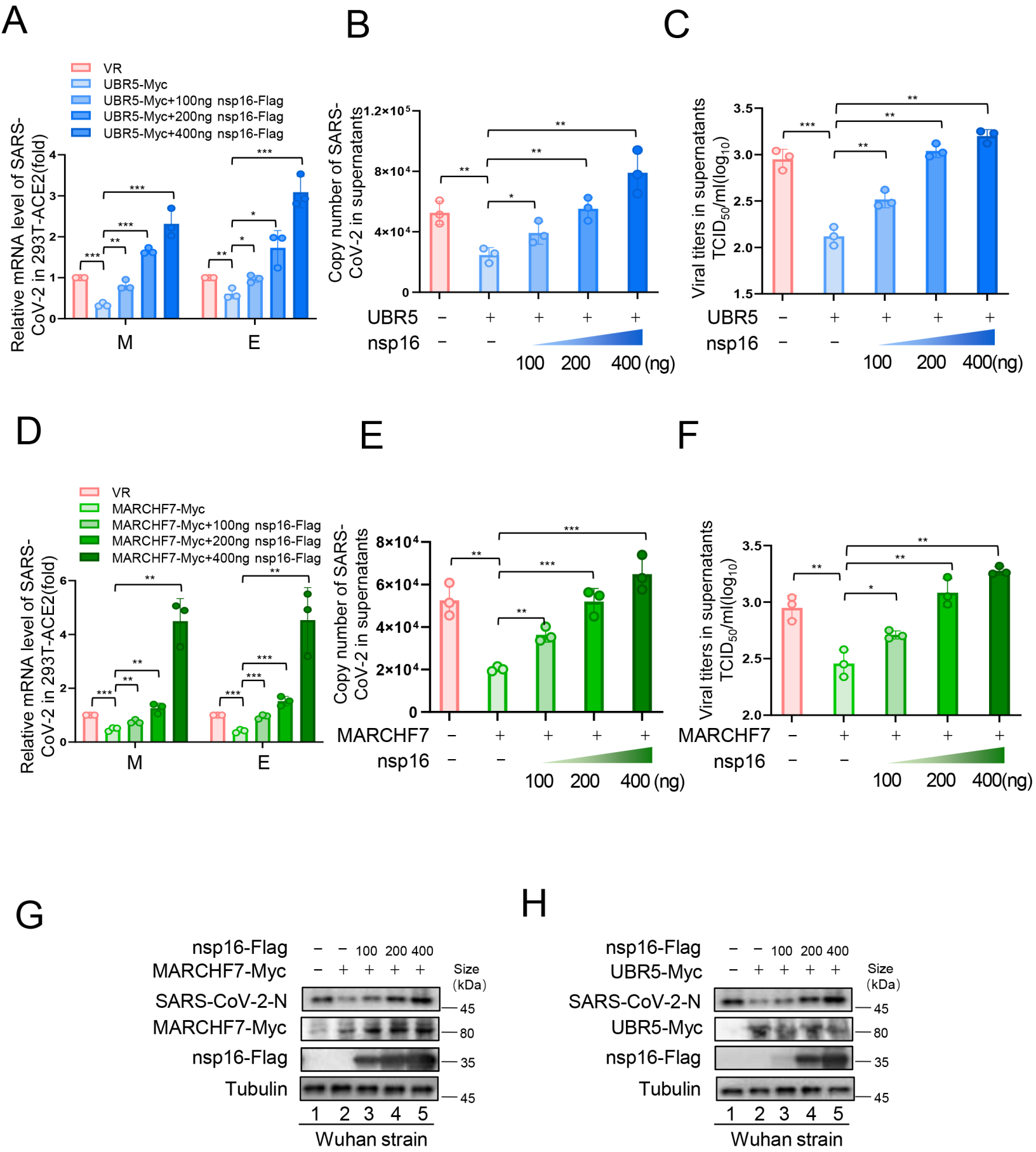
A
VR
UBR5-Myc
UBR5-Myc+100ng nsp16-Flag
UBR5-Myc+200ng nsp16-Flag
UBR5-Myc+400ng nsp16-Flag
Relative mRNA level of SARS-CoV-2 in 293T-ACE2(fold)
M
E
B
Copy number of SARS-CoV-2 in supernatants
UBR5
nsp16
100 200 400 (ng)
C
Viral titers in supernatants TCID50/ml(log10)
UBR5
nsp16
100 200 400(ng)
D
VR
MARCHF7-Myc
MARCHF7-Myc+100ng nsp16-Flag
MARCHF7-Myc+200ng nsp16-Flag
MARCHF7-Myc+400ng nsp16-Flag
Relative mRNA level of SARS-CoV-2 in 293T-ACE2(fold)
M
E
E
Copy number of SARS-CoV-2 in supernatants
MARCHF7
nsp16
100 200 400 (ng)
F
Viral titers in supernatants TCID50/ml(log10)
MARCHF7
nsp16
100 200 400(ng)
G
nsp16-Flag
MARCHF7-Myc
100 200 400
Size (kDa)
SARS-CoV-2-N
MARCHF7-Myc
nsp16-Flag
Tubulin
45
80
35
45
1 2 3 4 5
Wuhan strain
H
nsp16-Flag
UBR5-Myc
100 200 400
Size (kDa)
SARS-CoV-2-N
UBR5-Myc
nsp16-Flag
Tubulin
45
80
35
45
1 2 3 4 5
Wuhan strain

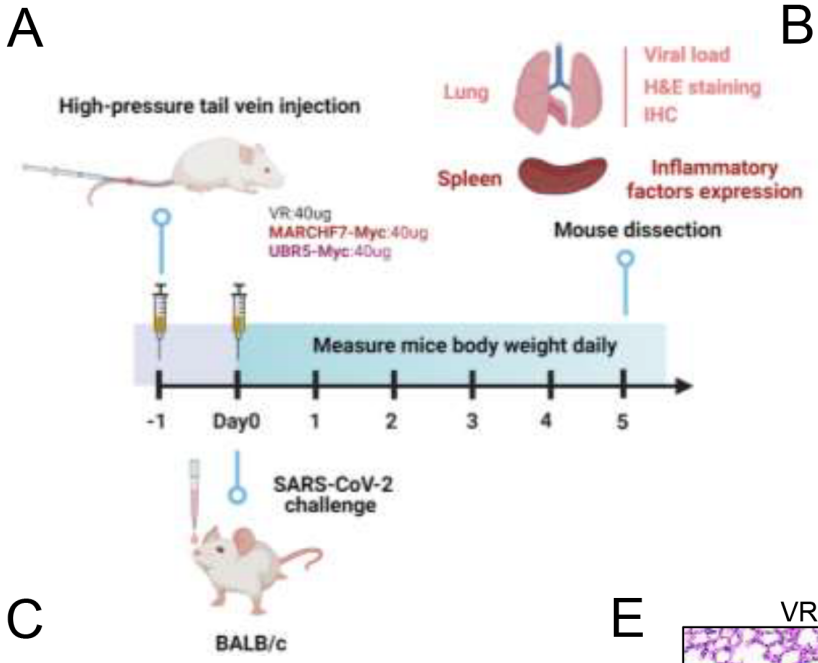
A
High-pressure tail vein injection
Lung
Viral load
H&E staining
IHC
Spleen
Inflammatory factors expression
VR:40ug
MARCHF7-Myc:40ug
UBR5-Myc:40ug
Mouse dissection
Measure mice body weight daily
-1
Day0
1
2
3
4
5
SARS-CoV-2 challenge
BALB/c

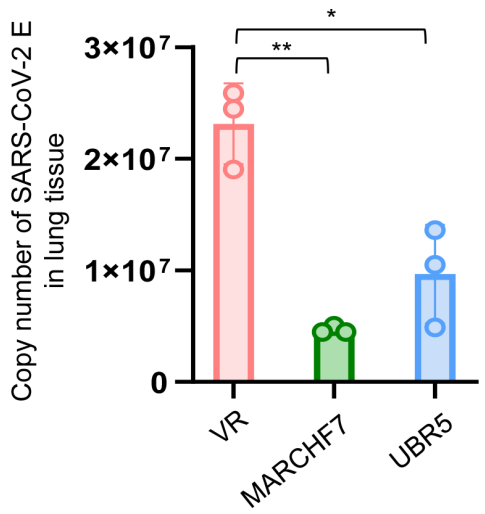
B
Copy number of SARS-CoV-2 E in lung tissue
3×10⁷
2×10⁷
1×10⁷
0
*
**
VR
MARCHF7
UBR5

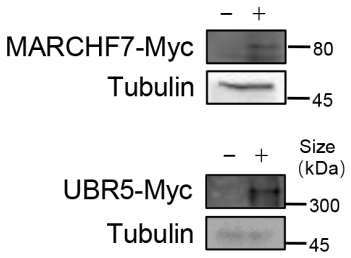
C
MARCHF7-Myc
Tubulin
80
45
UBR5-Myc
Tubulin
Size (kDa)
300
45

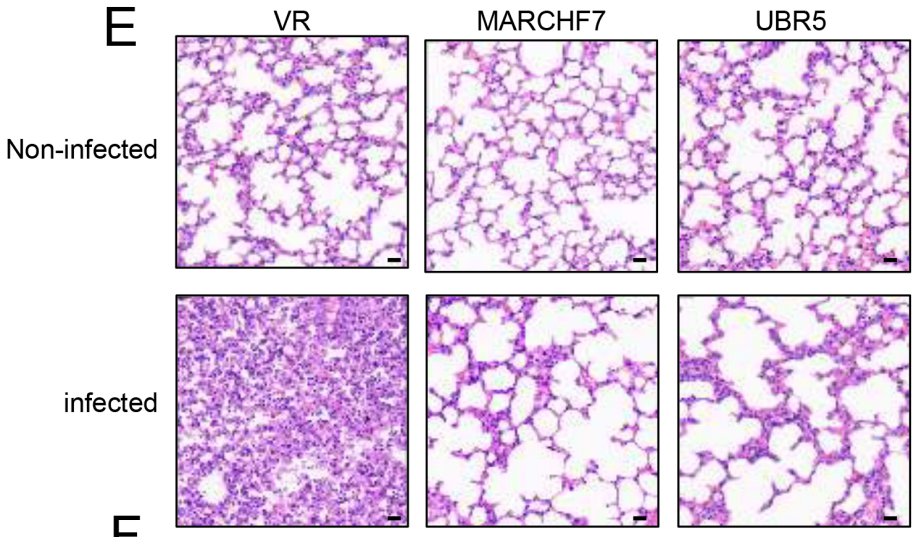
E
VR
MARCHF7
UBR5
Non-infected
infected

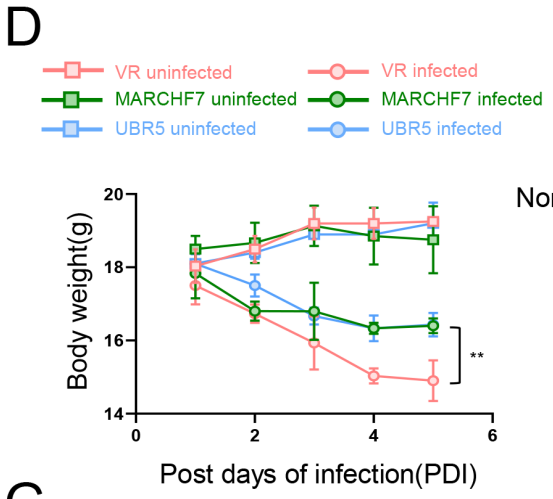
D
VR uninfected
VR infected
MARCHF7 uninfected
MARCHF7 infected
UBR5 uninfected
UBR5 infected
Body weight(g)
20
18
16
14
0
2
4
6
**
Post days of infection(PDI)

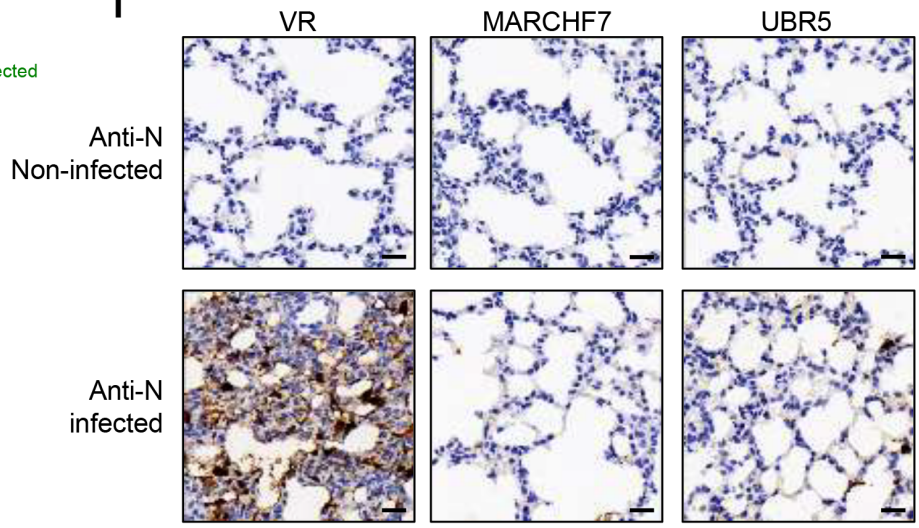
F
VR
MARCHF7
UBR5
Anti-N Non-infected
Anti-N infected

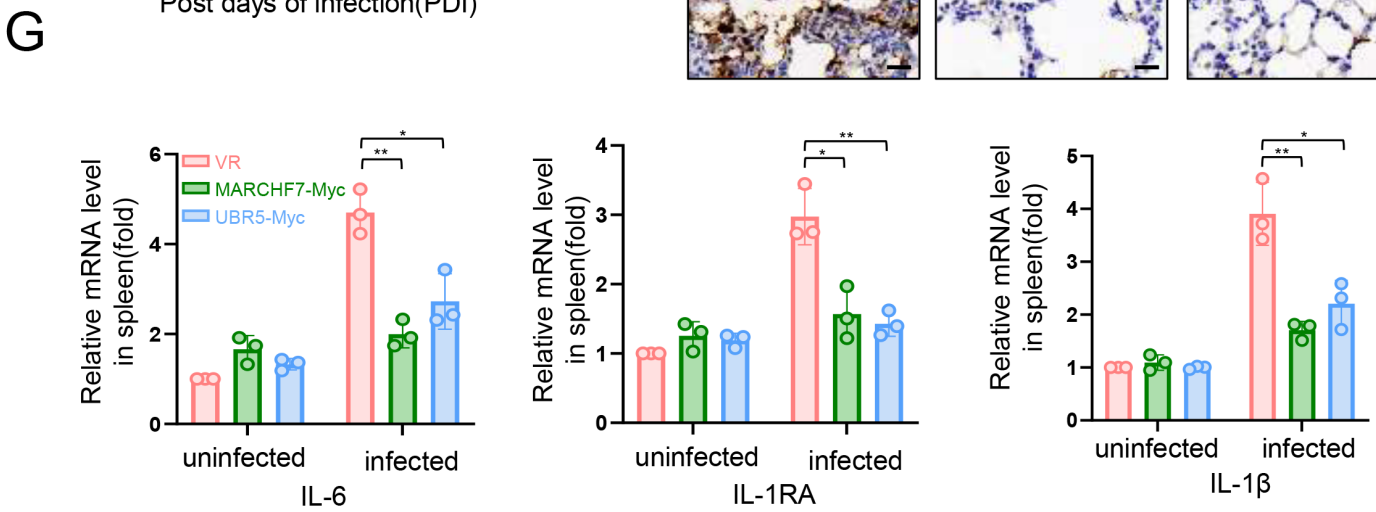
G
VR
MARCHF7-Myc
UBR5-Myc
Relative mRNA level in spleen(fold)
uninfected
infected
IL-6
IL-1RA
IL-1β

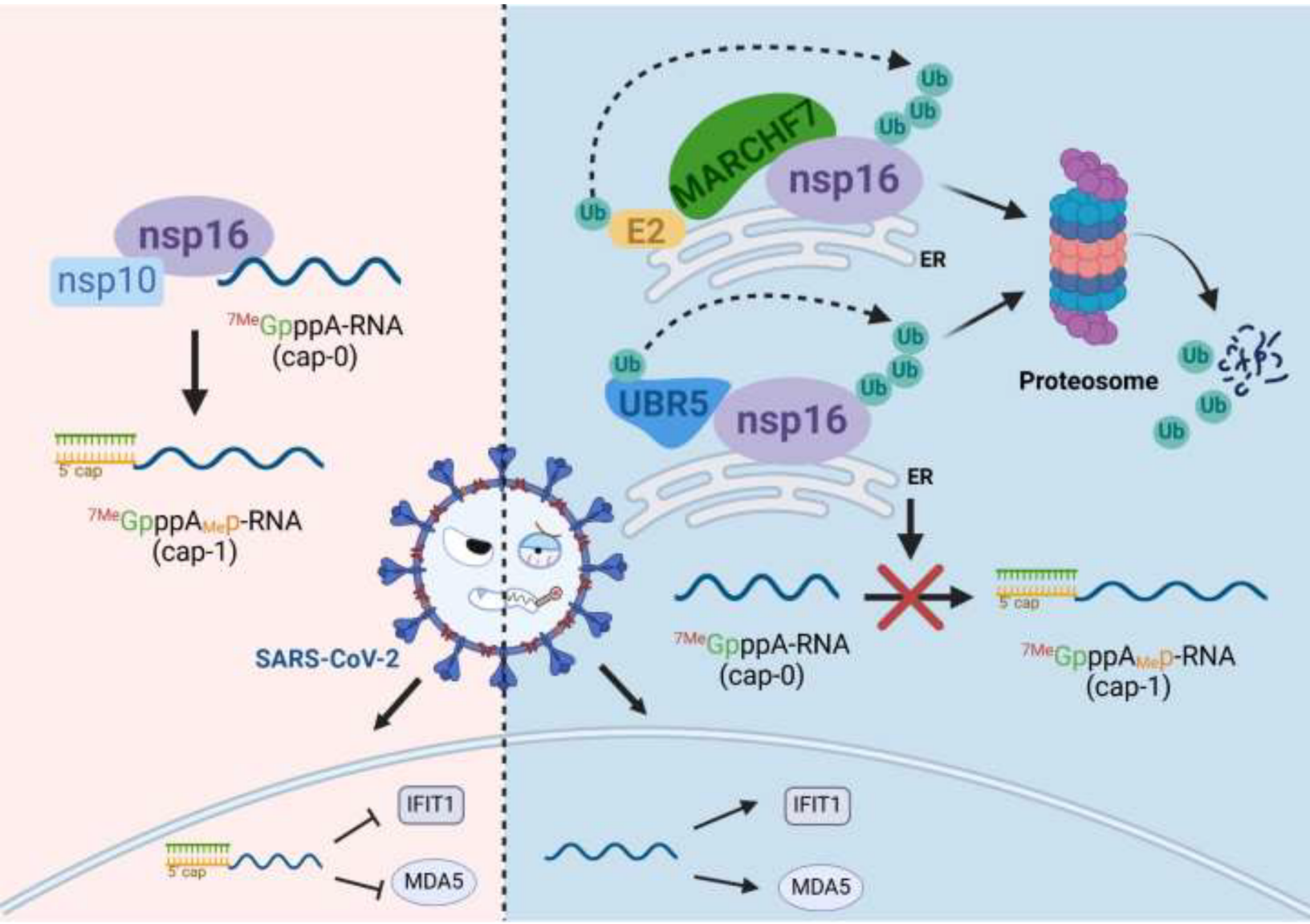
nsp16
nsp10
7MeGpppA-RNA
(cap-0)
5' cap
7MeGpppAMeP-RNA
(cap-1)
SARS-CoV-2
IFIT1
MDA5
5' cap
MARCHF7
nsp16
Ub
E2
ER
UBR5
nsp16
Proteosome
ER
7MeGpppA-RNA
(cap-0)
5' cap
7MeGpppAMeP-RNA
(cap-1)
IFIT1
MDA5